Manuscript Details

Manuscript number	JLP_2017_826
Title	A Priori Validation of CFD Modelling of Hydrocarbon Pool Fires
Article type	Full Length Article

Abstract

Fires can be an important hazard for the safety of chemical and process industries. Particularly, pool fires are the most frequent fire scenarios in such facilities and can affect other equipment of the plant with severe consequences due to the domino effect. During the last decades, simplified fire modelling tools were used to predict some of the harmful effects that hydrocarbon pool fires may entail. Although these can be applied to limited number of scenarios, they cannot cover the overall characteristics governing the fire behaviour. Computational Fluid Dynamics (CFD) modelling may provide more detailed insights of the related fire effects, may consider complex geometries and may represent from small to large-scale fires. However, simulation results should be firstly compared to experimental measurements in order to assess the predictive capabilities of these tools. This paper investigates the predictive capabilities of CFD modelling when performing a priori simulations of large-scale hydrocarbon pool fires. The main objective is to assess the fire effects prediction performance of two CFD codes that may be used to evaluate the hazard of hydrocarbon pool fires. FLACS-Fire and FDS codes have been used to simulate large-scale pool fires (1.5, 3, 4, 5 and 6 m-diameter) of diesel and gasoline fuels in unconfined environments. Given the notable differences between the mathematical methods applied to solve the CFD sub-models, the mesh resolution and the boundary conditions in each investigated tool, this study is not aimed at directly comparing both codes (i.e. using identical sub-models choices). However, the present CFD analysis is intended to reveal the potential of each software separately by applying the most appropriate modelling options for each tool. Based on a qualitative assessment of the predictions and a quantitative error estimation of the variables measured (i.e. flame temperature, burning rate, heat flux, flame height, flame surface, and surface emissive power), the main strengths and weaknesses of FLACS-Fire and FDS are identified when modelling hydrocarbon pool fires.

Keywords	Fire modelling; CFD; Pool fires.
Taxonomy	Chemical Engineering, Process Engineering, Process Safety
Corresponding Author	JOAQUIM CASAL
Order of Authors	Borja Rengel, Christian Mata, Elsa Pastor, JOAQUIM CASAL, Eulalia Planas

Submission Files Included in this PDF

File Name [File Type]

Highlights.docx [Highlights]

A priori validation of CFD modelling of hydrocarbon pool fires.docx [Manuscript File]

Figure 1.jpg [Figure]

Figure 2.jpg [Figure]

Figure 3.jpg [Figure]

Figure 4.jpg [Figure]

Figure 5.jpg [Figure]

Figure 6.jpg [Figure]

Figure 7.jpg [Figure]

Figure 8.jpg [Figure]

To view all the submission files, including those not included in the PDF, click on the manuscript title on your EVISE Homepage, then click 'Download zip file'.

Highlights

- Wind conditions and pool diameters resulted crucial factors that notably influenced the level of agreement of the predictions performed in both CFD codes.
- Simulated flames were usually higher and less tilted than in experiments and thus, numerous discrepancies were found when estimating the flame temperatures and heat fluxes received at a certain distance from the fire origin.
- The flame-geometry descriptors were successfully determined through a 2D slice file that registered the mean flame temperatures and a radiometer perpendicularly located to the predominant wind direction to measure the irradiancy.
- *A posteriori* simulations should be undertaken in order to figure out the most appropriate modelling options through a detailed sensitivity analysis.

A Priori Validation of CFD Modelling of Hydrocarbon Pool Fires

Borja Rengel, Christian Mata, Elsa Pastor, Joaquim Casal*, Eulàlia Planas

Centre for Technological Risk Studies (CERTEC), Department of Chemical Engineering
Universitat Politècnica de Catalunya, Eduard Maristany 10, 08019 Barcelona, Catalonia, Spain.
Joaquim.casal@upc.edu

Abstract

Fires can be an important hazard for the safety of chemical and process industries. Particularly, pool fires are the most frequent fire scenarios in such facilities and can affect other equipment of the plant with severe consequences due to the domino effect. During the last decades, simplified fire modelling tools were used to predict some of the harmful effects that hydrocarbon pool fires may entail. Although these can be applied to limited number of scenarios, they cannot cover the overall characteristics governing the fire behaviour. Computational Fluid Dynamics (CFD) modelling may provide more detailed insights of the related fire effects, may consider complex geometries and may represent from small to large-scale fires. However, simulation results should be firstly compared to experimental measurements in order to assess the predictive capabilities of these tools.

This paper investigates the predictive capabilities of CFD modelling when performing *a priori* simulations of large-scale hydrocarbon pool fires. The main objective is to assess the fire effects prediction performance of two CFD codes that may be used to evaluate the hazard of hydrocarbon pool fires. FLACS-Fire and FDS codes have been used to simulate large-scale pool fires (1.5, 3, 4, 5 and 6 m-diameter) of diesel and gasoline fuels in unconfined environments. Given the notable differences between the mathematical methods applied to solve the CFD sub-models, the mesh resolution and the boundary conditions in each investigated tool, this study is not aimed at directly comparing both codes (i.e. using identical sub-models choices). However, the present CFD analysis is intended to reveal the potential of each software separately by applying the most appropriate modelling options for each tool. Based on a qualitative assessment of the predictions and a quantitative error estimation of the variables measured (i.e. flame temperature, burning rate, heat flux, flame height, flame surface, and surface emissive power), the main strengths and weaknesses of FLACS-Fire and FDS are identified when modelling hydrocarbon pool fires.

Keywords: Fire modelling, CFD, Pool fires.

1. Introduction

Among the accidents occurring in chemical and process industries, fires are the most common types of events (Calvo Olivares et al., 2015, 2014). Precisely, large-scale pool fires (> 1 m-diameter) resulting from ignition of flammable liquid are the most frequent fire scenarios (Vasanth et al., 2013). Apart from the severe air pollution due to the release of unburned hydrocarbons and smoke into the atmosphere, pool fires can also trigger more severe effects with potential to threaten humans and structures (Pula et al., 2005). In general, pool fires occurring in industrial accidents are characterized by buoyancy-driven turbulent diffusion flames on a horizontal pool of fuel that is vaporized. The liquid pool mainly receives heat from the flames by convection and radiation. Once the fire has reached the steady state, the radiative heat transfer from flames to the fuel surface controls the fuel mass evaporation rate (Pedersen, 2012). In fact, the evaporation rate, which is a function of the pool diameter, and the resulting heat release rate are the main key variables in predicting pool fire effects (Wahlqvist and Hees, 2016). Additionally, large-scale hydrocarbon pool fires release considerable amounts of soot that may affect the overall thermal heat transfer as it may absorb and/or emit radiated heat from flames (Casal, 2017).

Within this framework, forecasting the pool fire effects may significantly contribute to prevent major fire accidents in chemical and process industries. Indeed, the radiative heat fluxes released and the high temperatures achieved may lead to structures collapse and/or severe hazard to people (Vianna and Huser, 2010). In this regard, fire risk assessments can identify the measures that should be implemented to eliminate and/or mitigate the fire impact (*Guidance on Risk Assessment for Offshore Installations*, 2006). Particularly, fire modelling techniques may be used to assess the fire risks and design protection measures rather than standard solutions (Baalisampang et al., 2017).During the last decades, simplified fire modelling tools were used to predict the harmful effects of hydrocarbon pool fires, which were commonly derived from specific sets of well-defined experiments and/or empirical correlations. Accordingly, these methods cannot cover the overall characteristics governing the fire behaviour and their range of applicability are restricted to a certain number of fire scenarios (Azzi and Rogstadkjenet, 2016).On the other hand, Computational Fluid Dynamics (CFD) modelling may provide more detailed insights of the related fire effects, may consider additional complexity, such as different geometries and alternative boundary conditions, and may represent different fire sizes: from small to large-scale fires. However, simulation results should be firstly compare against experimental measurements to assess the predictive capabilities of these modelling tools when determining the hazardous fire effects in open environments.

Validation of numerical codes, which consist in a comparison process between experimental and predicted data, is a necessary first step before their use in real applications. It determines the appropriateness of the governing equations to represent the physical phenomena of interest and allows the model amelioration from the disparities reached (McGrattan and Miles, 2016). In *a priori* CFD validation analysis, the user has no information about the experimental results and has access only to a brief description of the initial scenario (Torero et al., 2009). Accordingly, simulations cannot be 'tuned' to improve the results accuracy and the user is the only responsible for developing appropriate settings and assumptions. In addition, *a priori* or blind CFD simulations are commonly performed in fire risk assessments as the modeller has to examine the possible fire scenarios that could occur under different boundary conditions (Fu et al., 2016). Consequently, a validation analysis involving blind CFD simulations is doubly necessary: i) to assess the accuracy of the CFD codes used; and ii) to quantify the uncertainties that can be reached when performing this type of large-pool fire simulations.

This paper investigates the predictive capabilities of CFD modelling when performing *a priori* simulations of large-scale hydrocarbon pool fires. The main objective is to assess the fire effects prediction performance of two CFD codes that may be used to evaluate the hazard of hydrocarbon pool fires. FLACS-Fire and FDS codes have been used to simulate large-scale pool fires (1.5, 3, 4, 5 and 6 m-diameter) of diesel and gasoline fuels in unconfined environments. Given the notable differences between the mathematical methods applied to solve the CFD sub-models, the mesh resolution and the boundary conditions in each investigated tool, this study is not aimed at directly comparing both codes (i.e. using identical sub-models choices). However, the present CFD analysis is intended to reveal the potential of each software separately by applying the most appropriate modelling options for each tool. Based on a qualitative assessment of the predictions and a quantitative error estimation of the variables measured (i.e. flame temperature, burning rate, heat flux, flame height, flame surface, and surface emissive power), the main strengths and weaknesses of FLACS-Fire and FDS are identified when modelling hydrocarbon pool fires. This paper is organized as follows: Section 2 presents the pool fire experiments and the measurements performed; Section 3 describes the CFD models used and the modelling

options assumed; Section 4 illustrates the experimental and simulation results found; finally, Section 5 presents conclusions.

2. Experimental set-up

CFD simulations considered the large-scale pool fires performed in the Can Padró Safety Training Center (Barcelona, Spain) (Muñoz et al., 2004). As summarized in Table 1, the experiments were carried out using gasoline and diesel as fuel lying on top of a thin layer of water in five concentric circular pools made of reinforced concrete (1.5, 3, 4, 5 and 6 m-diameter).

Table 1: Main features of the large-scale pool fire experiments performed. Diameter and radiometer distances are in m; wind speed in m·s^{-1}, and ambient temperature in ºC.

Experiment	Fuel	Diameter	Wind speed	Ambient temperature	Radiometer distance	
					Axial	*Radial*
22_D15	Diesel	1.5	1.33	22	1.5	7.5
21_G15	Gasoline	1.5	0.44	20	1.5	7.5
01_D3	Diesel	3.0	2.39	12	0.1	9.0
17_G3	Gasoline	3.0	1.14	14	1.5	9.0
04_D3	Diesel	3.0	0.00	16	0.1	15.0
03_G3	Gasoline	3.0	0.00	13	0.1	15.0
14_D4	Diesel	4.0	0.43	20	0.1	12.0
13_G4	Gasoline	4.0	0.52	19	0.1	12.0
10_D5	Diesel	5.0	1.02	16	1.0	15.0
08_G5	Gasoline	5.0	0.00	19	0.1	15.0
07_D6	Diesel	6.0	1.10	19	0.1	18.0
06_G6	Gasoline	6.0	0.00	18	0.1	18.0

Different measuring devices were used to record the main variables related to fire behaviour. The weather conditions were obtained using a meteorological station located at 10 m height. The values found were averaged during the steady state phase. A set of five K-type thermocouples (3 mm-diameter) were located in the pool centreline axis to measure the flame temperatures at different heights over the fuel layer: 2.84 m (TB1), 3.96 m (TB2), 5.53 m (TB3), 6.96 m (TB4) and 11.01 m (TB5). A radiometer (RD), whose axial and radial distance to the pool origin was varied according to the experiments performed, was located opposite to the wind direction to measure the irradiance received at a certain distance. Burning rates were determined indirectly by means of a system of communicating vessels that measured weight loss (Chatris et al., 2001). Apart from the 03_G3 and 04_D3 experiments, the pool fires were filmed using a VHS camera, which registered visible images (Figure 1a), and a commercial thermographic IR camera, which was able to represent the apparent temperature distribution of the flame (Figure 1b). Both were placed together perpendicular to the predominant wind direction at different distances from the fire origin depending on the pool diameter to record the structure of the flame. For each test, the recorded IR images corresponding to the stationary state of the fire were lately treated with fan in-house MATLAB algorithm. It carried out a segmentation process to differentiate the flame region from the smoke plume by setting up a boundary temperature of 330ºC (Audouin et al., 1995; Cox and Chitty, 1980). Consequently, the evolutions of the flame height (H_F, m) and the flame surface (A_F, m^2) over time were established for each pool fire experiment (Figure 1c). Particularly, the flame height for each image was determined as the maximum distance between the pool base and the highest pixel element at a minimum temperature of 330ºC (Cowley and Johnson, 1991; Maragkos et al., 2017).

Furthermore, the surface emissive power (SEP), which represents the radiative heat flux at the surface area of the flames, was obtained by considering the temperature of each element (i.e. each pixel on the thermographic image) and the emissivity established as follows:

$$SEP_{i,j} = \varepsilon \cdot \sigma \cdot T_{i,j}^4 \quad (1)$$

where $T_{i,j}$ is the temperature (K) of a pixel element, i and j indicate the position of the pixel in the IR image, $SEP_{i,j}$ is the surface emissive power (kW·m^{-2}) of the pixel element, ε is the emissivity, and σ is the Stefan-Boltzmann constant (kW·K^{-4}·m^{-2}). As hydrocarbon pool fires become optically thick at diameters of ~ 3 m (Planas-Cuchi et al., 2003), the following emissivity values were adopted according to the pools sizes: 0.95 for

diameters of 1.5 m, 0.98 for 3 m, and 1 for diameters equal or higher than 4 m. Then, the time averaged surface emissive power of a pixel element during the steady state can be calculated by:

$$\overline{SEP}_{i,j} = \frac{\sum_1^{N_T} SEP_{i,j}}{N_T} \quad (2)$$

where N_T represents total images in the thermographic sequence investigated. Finally, the mean surface emissive power of the total flame is written as:

$$\overline{SEP} = \frac{\sum_i \sum_j \overline{SEP}_{i,j} \cdot a_x}{\sum_i \sum_j a_x} \quad (3)$$

where a_x is the area of a pixel in the infrared image (m^2).

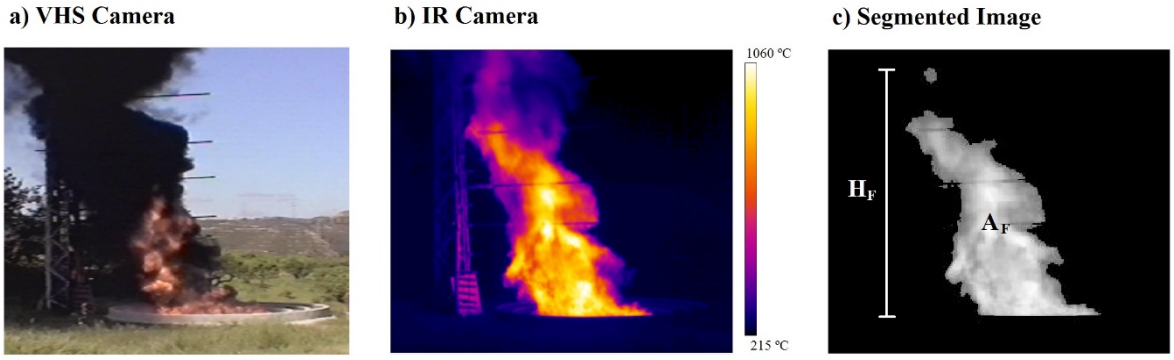

Figure 1: Example of video images recorded during the stationary state of the 01_D3 fire experiment by means of a) the VHS camera, b) the IR camera and c) the corresponding segmentation process applied to obtain the flame height (H_F), and surface (A_F).

3. Numerical modelling

Fire Dynamics Simulator v6.5.3 (FDS) (McGrattan et al., 2015) developed by National Institute of Standards and Technology (NIST) and Flame Accelerator Simulator Fire v10.6 (FLACS-Fire) (*FLACS v10.5 User's Manual*, 2016) developed by Gexcon AS were used to simulate the experimental pool fires. FDS is an open source code intended to represent fire driven fluid flows that numerically solves a form of the Navier-Stokes equations appropriate for low-speed, thermally-driven flow, with an emphasis on smoke and heat transport from fires. Conversely, FLACS-Fire is a commercial CFD code specially built for quantitative risk assessment applications related to fire hazards in the process industry. All numerical simulations were set to run for 150 s. Following sections describe the sub-models employed for both CFD tools, the mesh resolution, the boundary conditions and the measuring devices that were set up to run simulations.

3.1 CFD Sub-models

3.1.1 Turbulence

In order to describe the mixing phenomenon of the fluid, FLACS-Fire considers the Reynolds Averaged Navier–Stokes (RANS) (Jones and Launder, 1972) turbulence model, whereas FDS represents the flow motion by means of the Large Eddy Simulations (LES) (Smagorinsky, 1963). The RANS approach solves the Navier-Stokes equations for the mean flow variables and only computes the large scale motions. Because of its simplicity and low computing requirements, RANS has been widely used in industrial CFD applications during the last years. Nevertheless, the limitations of the RANS model when simulating the highly oscillating buoyancy-induced flow have been already recognised (Sapa et al., 2010). On the other hand, LES filters out the small eddies of the flow and provides a more realistic-looking flow field than the time-averaged RANS model in a reasonable computing time. However, one of the main drawbacks of LES is that the modeller should pay close attention to the choice of numerical grid as the accuracy of the simulation may be degraded if there are not enough grid cells to describe the flow field (McGrattan and Miles, 2016).

3.1.2 Pyrolysis

In *a priori* CFD simulations the fuel mass loss rate is unknown and thus, it should be predicted by means of the pyrolysis models implemented in the codes used. Prior to ignite liquids, the evaporation process of fuel should generate a certain volume of flammable vapour fuel over the liquid layer. In FLACS-Fire, the liquid evaporation rate is determined through a heat transfer balance dominated by the heat from the flame, the sun, and the substrate. In addition, a ground temperature of 490 K and 341 K was selected for the diesel and gasoline pools, respectively, which coincides with the boiling temperatures of each compound, to facilitate the formation of the combustible cloud. After a while, a source of heat was settled just above the liquid area to allow the ignition of the fire. On the other hand, the liquid evaporation rate in FDS is a function of the liquid temperature and the fuel vapour pressure above the fuel layer as presented by Sikanen and Hostikka (Sikanen and Hostikka, 2016). Regardless of the fuel layer in-depth, the liquid is treated as a thermally-thick solid in order to consider the heat conduction within the pool. The evaporation model directly allowed the flame ignition of gasoline pools due to its low boiling temperature, whereas a hot static particle at 500 ºC remained during a short period of time above the diesel pools in order to ignite the combustible gases.

3.1.3 Combustion

The products released from the chemical reaction of fuel vapour and oxygen were quantified through the Eddy Dissipation Concept (EDC) (Magnussen and Hjertager, 1977) and the Mixture Fraction (MF) (Floyd et al., 2001) combustion models for FLACS-Fire and FDS, respectively. The EDC model is a simple and robust model that requires a lot of processing power. Also, it neglects many of the processes related to turbulence dynamics and does not detail the chemistry necessary for the calculation of emissions. The MF model solves the species transport based on an infinitely fast reaction of fuel and oxygen that only allows one single gaseous fuel resulting from the combustion process. It combines the transport equations into a single one to reduce the computational cost, which neglects all the intermediate combustion products released.

During the gas-phase combustion, the formation of soot may significantly affect the heat transfer process, especially due to its capacity to absorb and/or emit part of the radiative energy from the flame. Even though there exist several detailed models intended to calculate the formation and growth of soot from large fires, most of these require some form of adjustment to provide reasonable predictions. Because of that, a simplified model that converts a certain fraction of fuel carbon into soot directly was chosen for both CFD tools as it reduces the derived uncertainties of complex soot models and the computational costs. The soot and carbon monoxide yield values were selected according to the fuel properties (Koseki, 1999). Moreover, the thermal properties of diesel (Sikanen and Hostikka, 2017) and gasoline (Sudheer, 2013) were defined to compute the pyrolysis and the reaction of combustion as shown in Table 2.

Table 2: Thermal properties of the pool liquid fuels required to solve the pyrolysis and the reaction of combustion.

Parameter	Units	Diesel	Gasoline
Pyrolysis			
Density	$Kg \cdot m^{-3}$	749	750
Specific heat	$kJ \cdot kg^{-1} \cdot K^{-1}$	2.4	2.06
Conductivity	$W \cdot m^{-1} \cdot K^{-1}$	0.18	0.11
Absorption coefficient	m^{-1}	300	200
Heat of combustion	$kJ \cdot kg^{-1}$	380	317
Heat of reaction	$MJ \cdot kg^{-1}$	42	44.4
Boiling temperature	ºC	215.8	68
Reaction of Combustion			
Chemical formula	-	$C_{12}H_{26}$	C_6H_{14}
Soot yield	$kg \cdot kg^{-1}$	0.10	0.10
Carbon monoxide yield	$kg \cdot kg^{-1}$	0.012	0.010

3.1.4 Radiation

CFD codes include different advanced mathematics techniques to solve the radiative transfer equation (RTE), which describes the radiation intensity field in an absorbing, emitting and scattering medium. Particularly, FLACS-Fire uses the discrete transfer method (DTM) (Shah, 1979), while FDS employs the finite volume method (FVM) (Chai et al., 1994). Both approaches largely depend on the number of solid angles configured to solve the radiative transfer equation when running fire simulations. In general, the higher the number of solid angles implemented, the higher the accuracy of the heat fluxes predicted and the longer the computational times

required to complete simulations. In the present validation analysis, 100 solid angles were selected for simulations in both CFD codes.

3.2 Mesh resolution

The computational domains were composed by rectangular and isotropic grid cells that varied according to the experimental tests simulated. For simulations involving buoyant plumes, the non-dimensional expression D^*/δ_x is recommended to measure how well the fluid flow field is resolved as follows (Lin et al., 2010):

$$D^* = \left(\frac{\dot{Q}}{\rho_\infty \cdot c_p \cdot T_\infty \cdot \sqrt{g}}\right)^{(2/5)} \quad (4)$$

where D^* is the characteristic diameter of the fire in m; δ_x is the nominal size of a mesh cell; $\dot{Q}$ is the total heat release rate of the fire expressed in kW; ρ_∞ is the ambient density in kg·m^{-3}; c_p is the specific heat in kJ·kg^{-1}·K^{-1}; T_∞ is the ambient temperature in K; and g is the gravity in m·s^{-2}. The quantity D^*/δ_x can be seen as the number of grid cells spanning the characteristic diameter of the fire. Concerning the heat release rate of the fire, it can be defined by means of the following correlation:

$$\dot{Q} = \dot{m}'' \cdot A \cdot \Delta H_c \quad (5)$$

where $\dot{m}''$ is the mass loss rate of a given fuel in g·m^{-2}·s^{-1}; A is the pool area measured in m^2; and ΔH_c is the heat of reaction of the pool fuel. As recommended, the values of the correlation should be ranged between 4 (coarse cells size) and 16 (thin cell size) for being solved adequately (Sally and Kassawara, 2007). Considering the mass loss rates of gasoline and diesel pools obtained in previous works (Muñoz et al., 2004), and depending on the pool diameter and the δ_x parameter, cell grid sizes varied from 0.10 to 1.20 m approximately.

In general, the higher number of cells contained in the characteristic diameter, the longer the computational times and the higher the calculation resolution. In the case of FLACS-Fire, it can only run simulations with a mesh that fills the entire volume, as it employs a single CPU core to process the computational calculations. Accordingly, a uniform cell size of 0.2 m per side was selected to run simulations in a reasonable computational time (Table 3). On the other hand, the domain modelled in FDS can be divided in multiple meshes contained in different CPU cores in order to accelerate the simulation progress. The amount and location of the meshes considered in the fire scenarios simulated varied according to the fire experiment simulated and the boundary conditions established. Particularly, FDS simulations were set up with a cell size of 0.10 m per side in the pool base to increase the burning rate calculation resolution with additional greater meshes of 0.20 m per side covering the rest of the volume. Moreover, squared-pool bases were drawn in FDS simulations because of the use of Cartesian grid cells, whereas round-pool base geometries were used for FLACS-Fire as it incorporates the porosity concept. (i.e. it represents the fraction of the area or volume that is accessible for a fluid to flow, which can be featured from 0 (the volume is completely blocked) to 1 (the volume is completely open).

Table 3: Computational domain and number of cells considered for the fires simulated with FDS and FLACS. Computational domain in m^3.

Simulation	Computational Domain	Number of cells	
		FDS	***FLACS-Fire***
22_D15	12.5 x 8 x 14	≈ 730,000	≈ 180,000
21_G15	12.5 x 8 x 14	≈ 730,000	≈ 180,000
01_D3	15 x 10 x 16	≈ 1,100,000	≈ 300,00
17_G3	15 x 10 x 16	≈ 850,000	≈ 300,00
04_D3	21 x 10 x 16	≈ 1,500,000	≈ 420,000
03_G3	21 x 10 x 16	≈ 1,500,000	≈ 420,000
14_D4	19 x 12 x 18	≈ 1,700,000	≈ 500,000
13_G4	19 x 12 x 18	≈ 1,700,000	≈ 500,000
10_D5	22.5 x 13 x 22	≈ 2,100,000	≈ 800,000
08_G5	22.5 x 13 x 22	≈ 2,100,000	≈ 800,000
07_D6	26 x 14 x 25	≈ 2,640,000	≈ 1,140,000
06_G6	26 x 14 x 25	≈ 2,640,000	≈ 1,140,000

3.3 Boundary conditions

Given the nature of the experiments, the computational boundaries were opened to the outside hence allowing the external flow to enter and to leave the domain. The *Nozzle* and the *Open* vents formulations were applied in FLACS-Fire and FDS boundaries, respectively. As seen in the experimental set-up description, most of the experiments were undertaken under the presence of low wind. Actually, there exist various numerical methods to reproduce wind conditions. In the case of FLACS-Fire, the software considers the approach of Monin-Obukhov (Monin and Obukhov, 1959), which developed a mathematical model to determine the buoyancy effects on the atmospheric boundary layer. In a different way, the atmospheric wind profile was used in FDS as it seems suitable for fire scenarios in opened environments. Furthermore, the ground roughness, which refers to the aerodynamic roughness length, may notably influence the fire behaviour simulations in the presence of wind. In both CFD codes a ground roughness of 0.25 m was chosen for the unconfined simulations in grass terrains (Möller, 1973).

3.4 Measuring devices

Temperatures and radiative heat fluxes were measured in both CFD tools via thermocouples and a radiometer located as described in the experimental set up, whereas the pool burning rates were directly computed by the software employed. In addition, a 2D slice file (SF) was positioned on the pool central axis of the ZX plane in order to register the inner flame temperature distribution (Figure 2). The described methodology applied during the experiments with the IR camera by setting up a boundary flame temperature of 330ºC was implemented in the fire simulations to obtain flame-geometry descriptors (i.e. flame height and flame surface). Moreover, an additional wide-angle radiometer (RD_SEP) was located at 4.5 m from the fire origin and 0.5 m above the ground perpendicular to the predominant wind direction in order to determine the mean surface emissive power of the flame by the following equation:

$$\overline{SEP} = \frac{\overline{E}}{\varphi_{F,R,max} \cdot \tau} \tag{6}$$

where $\overline{E}$ is the time averaged irradiance recorded for the RD_SEP radiometer (kW·m^{-2}), τ is the atmospheric transmissivity assumed to be 1, and $\varphi_{F,R,max}$ is the view factor from the flame (F) to the radiometer (R), which depends on the flame shape, the relative distance between the fire and the receiving element, and the relative orientation of the radiometer. For a vertical flame cylinder, the maximum view factor could be calculated as follows (Mishra, 2010):

$$b = \frac{y_{F,R}}{r_p};\ a = \frac{L_F}{r_p};\ A = (b+1)^2 + a^2;\ B = (b-1)^2 + a^2$$

$$\varphi_{F,R,h} = \frac{1}{\pi}\left(\tan^{-1}\sqrt{\frac{b+1}{b-1}} - \left(\frac{b^2-1+a^2}{\sqrt{AB}}\right)\tan^{-1}\sqrt{\frac{(b-1)A}{(b+1)B}}\right) \tag{7}$$

$$\varphi_{F,R,v} = \frac{1}{\pi}\left(\frac{1}{b}\tan^{-1}\frac{a}{\sqrt{b^2-1}} + \frac{a(A-2b)}{b\sqrt{AB}}\tan^{-1}\sqrt{\frac{(b-1)A}{(b+1)B}} - \frac{a}{b}\tan^{-1}\sqrt{\frac{(b-1)}{(b+1)}}\right) \tag{8}$$

$$\varphi_{F,R,max} = \sqrt{\varphi_{F,R,h}{}^2 + \varphi_{F,R,v}{}^2} \tag{9}$$

where $y_{F,R}$ is the distance between the fire origin and the radiometer (m), r_p is the pool radius (m), $\varphi_{F,R,h}$ and $\varphi_{F,R,v}$ are the horizontal and vertical view factors, respectively.

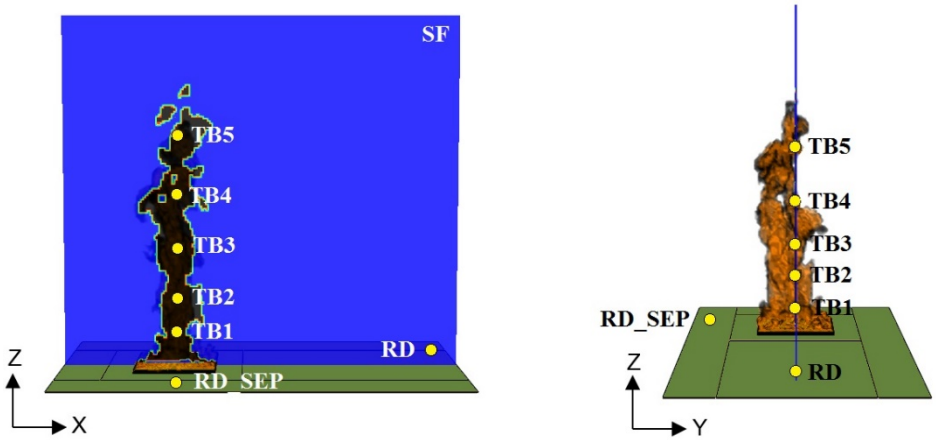

Figure 2: Example of a FDS simulation belonging to one instant of the steady state of the 14_D4 experiment where the location of measuring devices is shown. Thermocouples and radiometers are represented with round yellow dots while the slice file is represented with a 2D blue plane. Left image exposes the flame contour (black shadow) derived from the boundary flame temperature (330ºC), whereas the right image reveals the approximate flame volume.

4. Results and discussion

4.1 Experimental results

It is worth pointing out that some of the measurements collected during these experiments were previously used to analyse different characteristics of hydrocarbon pool fires (Ferrero et al., 2007, 2006; Muñoz et al., 2007, 2004). However, the current investigation discusses the whole set of data found in order to provide more in-depth understanding of these type of fires. The following scatter plots represent the mean values of the main variables of interest, which were obtained by averaging their evolutions over 30 s during the steady state phase. When possible, the experimental variables are expressed in dimensionless quantities to allow the comparison between different pool fire scales. For example, the mean flame height (H_F) is expressed as a function of the pool diameter (D); and the mean flame area ($A_{F)}$ as a function of the pool area (A_P). In addition, tendency lines are included to depict the different variable's evolutions as some parameters varied: power trend lines assess the centerline flame temperature at different heights, while linear trend lines analyze the influence of the pool diameters and wind velocity on the gasoline and diesel pool fires. Also, vertical bars are added to represent the measurements uncertainties around their mean values, which were calculated through the standard deviation as follows:

$$s^2 = \frac{\sum_1^n (X_0 - \overline{X})^2}{n-1} \tag{10}$$

where s is the standard deviation of the measurements, X_0 is a measured value along the complete set of data recorded, n is the number of total measured values, and $\overline{X}$ is the mean of the measured values.

Figure *3* shows the mean temperatures evolutions according to the thermocouples heights (L_T) and the pool diameter (D). Regarding the diesel pool fires, it is observed that three pool experiments with different diameters (22_D15, 01_D3, and 10_D5) register similar temperatures along the centerline axis (~40 ºC). In those cases, the lateral winds significantly tilt their flames and thus, the centerline thermocouples were not in contact with the fire plume. However, other diesel pools under the presence of wind (i.e. 14_D4 and 07_D6) achieved higher temperatures along the axis. Consequently, it is highlighted that wind significantly affects the mean centerline temperatures of diesel pools as flames may be tilted depending on the pool diameter and the wind velocity (Figure 4). In fact, the highest values registered are found in the absence of wind for the 04_D3 experiment. In general, it might be inferred that for each pool diameter there is a characteristic wind speed that inclines its flame hence modifying its height and area: the larger the pool diameter, the higher the characteristic wind speeds should be to overcome the buoyancy driven forces of the pool. Nevertheless, more research is still required in order to precisely determine these characteristics wind speeds as function of the diesel pool diameters.

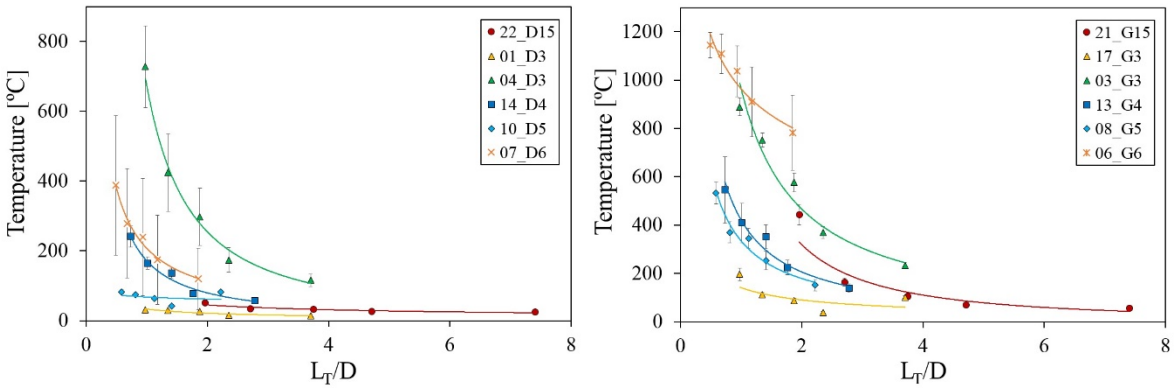

Figure 3. Mean flame temperatures measured during the steady state phase as a function of the thermocouples heights for the diesel pool fires (left) and the gasoline pool fires (right). Vertical error bars indicate the measurements uncertainties and power trend lines reveal the temperature evolution as the thermocouples heights vary.

Considering the difficulties of controlling the wind conditions, CFD modelling could be used to determine the velocities at which the flames become significantly tilted instead of performing experimental tests. Otherwise, it is generally observed that gasoline pools reach greater centerline flame temperatures than diesel fires under similar boundary conditions. For example, 3 m-diameter pool fires in the absence of wind achieve mean maximum temperatures of 900ºC and 750ºC when involving gasoline and diesel, respectively. The mean temperature differences between gasoline and diesel experiments could be due to the boiling temperatures of both fuels. As gasoline is featured with a lower boiling temperature than diesel, it requires less amount of heat to evaporate the liquid fuel. Accordingly, gasoline pools release a large amount of combustible gases that may contribute to complete the combustion process. Furthermore, it is noted that the measurements uncertainties commonly become more noticeable as the mean flame temperatures increase. Therefore, temperature results are less reliable when examined at lower flame regions, especially if there is no wind.

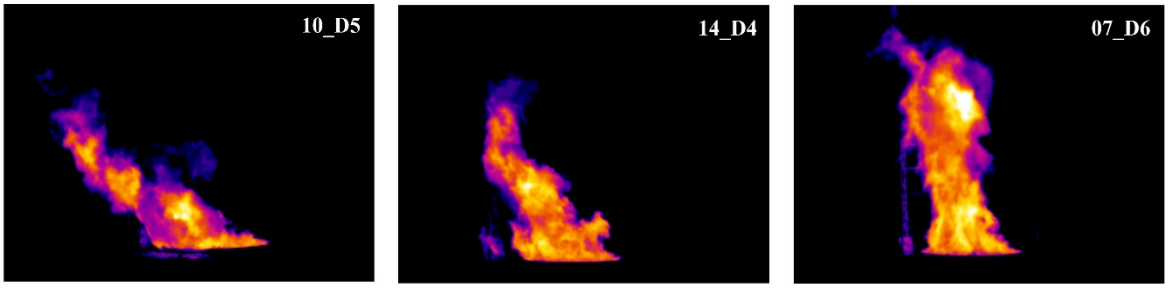

Figure 4. IR images belonging to one instant of the steady state of different experiments that reveal the flame tilt effect, which depends on the pool diameter and the wind velocity.

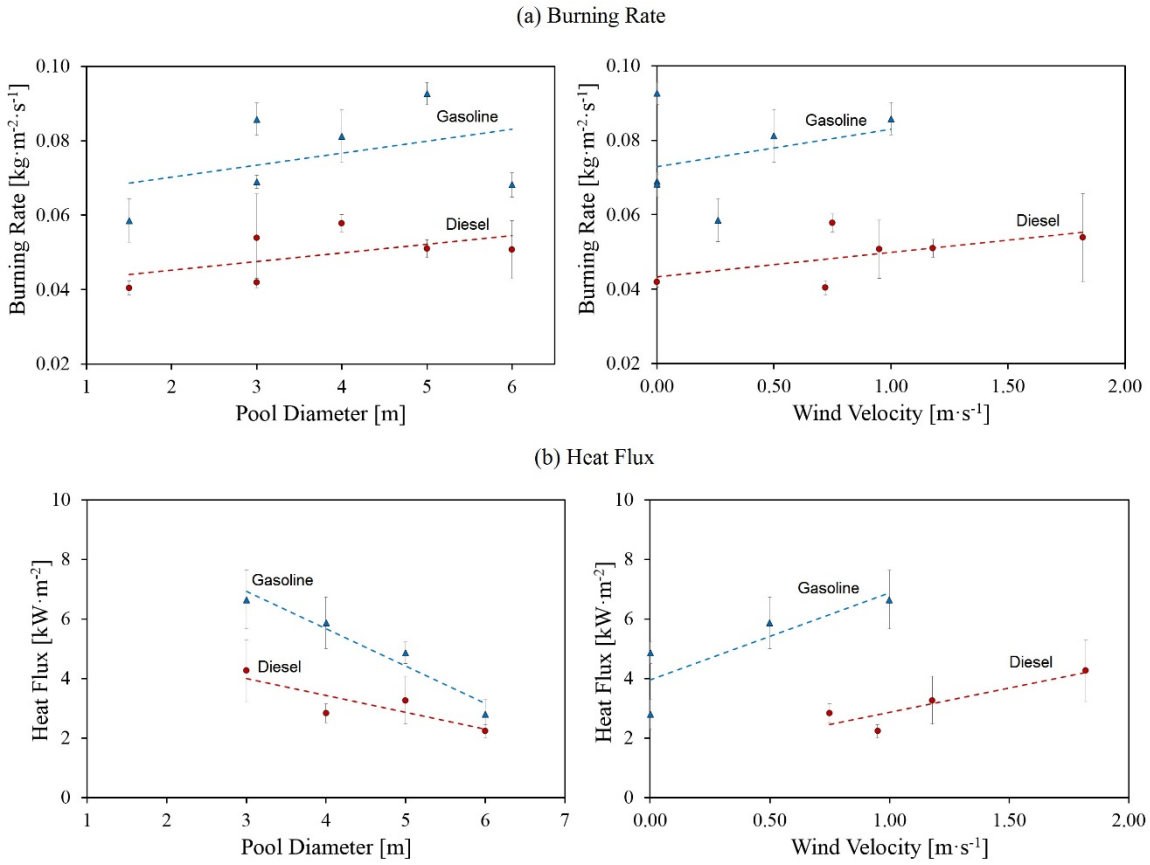

Figure 5. a) Mean burning rates measured and b) mean radiative heat fluxes received at a 5D m distance from the fire origin as a function of the pool diameter (left) and the wind velocity (right). Vertical error bars indicate

the measurements uncertainties and linear trend lines reveal the variables evolution as the pool diameters and wind velocities vary.

As occurred with the mean flame temperatures, higher burning rates are found in gasoline pool fires rather than diesel pools (Figure 5a). Particularly, the burning rate increases with the pool diameter and/or the wind velocity. On the other hand, the heat flux received at 5D m from the fire origin decreases as the pool diameter increases and thus, it may be noted that smaller pool fires release higher heat fluxes than bigger pool fires at the same relative distances from the fire origin (Figure 5b). In fact, it is deduced that the smoke blockage effect results more significant as the pool diameter increases. However, different pool sizes should be examined under similar wind conditions in order to clearly establish the influence of this phenomenon over the radiative heat flux. As previously noted, CFD modelling may be used to investigate its impact rather than large-scale experiments. Moreover, the higher wind velocities lead to greater heat fluxes measured by the radiometer. Furthermore, it is observed that neither the pool diameter nor the wind velocity have a notable influence over the burning rate and heat flux uncertainties. Indeed, significant measurements uncertainties may be achieved under different fire sizes and diverse boundary conditions.

(a) Flame Length

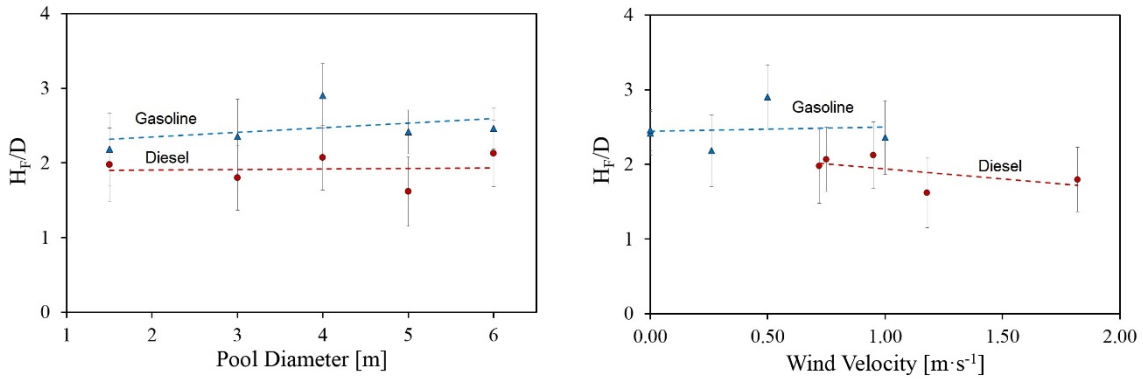

(b) Flame Area

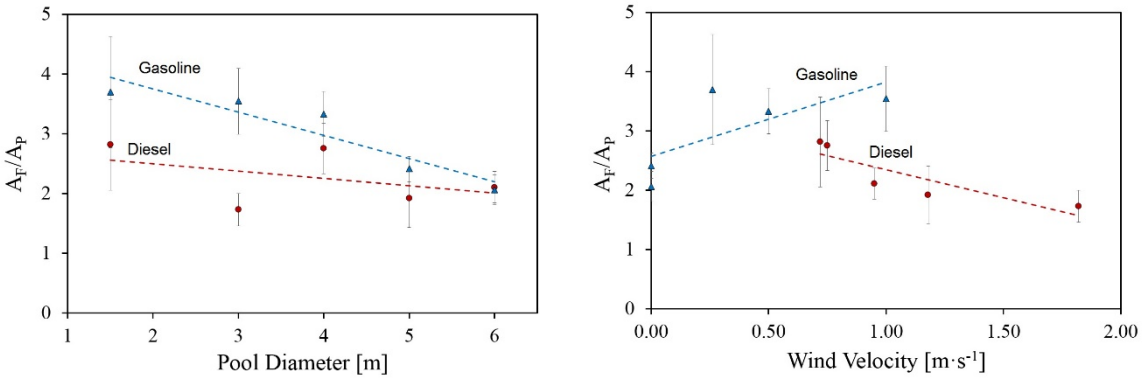

(c) Surface Emissive Power

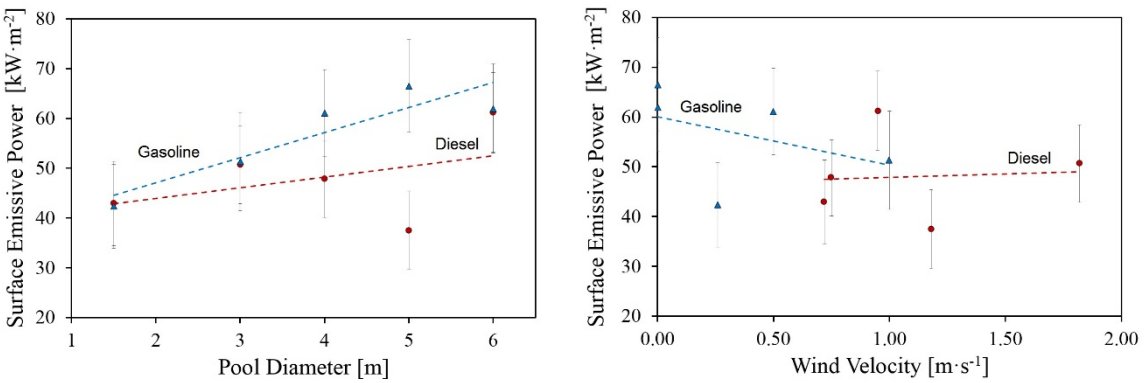

Figure 6. a) Mean flame height, b) mean flame areas and b) mean surface emissive powers calculated from the IR images as a function of the pool diameter (left) and the wind velocity (right). Vertical error bars indicate the measurements uncertainties and linear trend lines reveal the variables evolution as the pool diameters and wind velocities vary.

Concerning the flame-geometry descriptors obtained through the IR images, it is observed that gasoline and diesel pool fires are featured with an approximate dimensionless mean flame height of 2.5D and 1.9D m, respectively (Figure 6a). Accordingly, neither the pool diameter nor the wind velocity have a considerable influence over the flame height. Similarly, higher dimensionless mean flame areas are found in gasoline pool fires rather than in diesel fires (Figure 6b). However, the difference of areas between fuels decrease as the diameter increases. For example, the mean absolute difference between fuels when considering pool fires of 1.5 m-diameter is of $1.5A_p$ m^2, while 6 m-diameter pool fires lead to similar flame areas. Likewise, as the wind velocity increases, the area augments/diminishes in the case of gasoline/diesel pools, respectively. Contrarily, the mean surface emissive powers measured describe an opposite behaviour than the flame areas (Figure 6c). Particularly, both fuels are featured with similar mean SEP around 45 $kW \cdot m^{-2}$ for the 1.5 m-diameter pool fires, however, as the diameter increases the absolute difference between combustible pools augments. For example, pool fires of 6 m-diameter achieve a mean SEP of 65 $kW \cdot m^{-2}$ and of 50 $kW \cdot m^{-2}$ for gasoline and diesel fuels, respectively. Moreover, it is stated that gasoline fires reduce their mean SEP as the wind speed increases, while diesel pools tend to maintain a steady mean value around 48 $kW \cdot m^{-2}$. In addition, the uncertainties of the flame-geometry descriptors are considerably noticeable all over the pool diameters and wind velocities experimented. Accordingly, these deviations around the mean values indicate the high degree of sensitivity of the IR camera as the temperatures registered varied significantly during the steady state. As observed, the wind velocity plays an essential role in the flame areas and the surface emissive powers analyzed. Due to the difficulties in achieving a clear understanding of its influence, an in-depth CFD modelling investigation could depict the stated variables evolution as the wind varies.

4.2 CFD Modelling results

4.2.1 Qualitative assessment of the predictions

Despite the potential of CFD modelling tools to predict the evolution of the main variables of interest, the similarity between experimental measurements and simulations may be limited to a certain number of cases. In order to qualitatively assess the prediction performance of FDS and FLACS-Fire, the following figures illustrate the performance of FDS and FLACS-Fire when representing the main fire variables. The scatter plots represent the averaged values of these, which were obtained by averaging the simulation results over 30 s during the steady state phase. The solid diagonal lines indicate perfect agreement between simulated and experimental values, while the dotted lines and long-dashed lines represent the ±25 and ±50 % prediction error with regard to the measurements, respectively. All graph include vertical and horizontal bars that represent the standard deviation of the simulation results and the experiments, respectively.

In order to provide an overview of the predicted flame temperatures, these are obtained by averaging the mean values registered through the different thermocouples set up for each fire simulation (Figure 7a). In general, it is observed that a higher agreement is found in FLACS than in FDS. In particular, most of the mean flame temperatures predicted in FDS are notably over-estimated, which could be due to the low impact of the wind entrainment modelled on the fire plume. Consequently, the resulting flames are less tilted than in reality and thus, these remain in permanent contact with the thermocouples, which lead to greater temperature values than measured during the experiments. On the other hand, FLACS randomly under/over predicts the registered mean flame temperatures. For example, these are always under-estimated for pool fires of 3 m-diameter, while over predictions are reached when simulating 4 m-diameter pool fires. In addition, it is remarked that flame temperature uncertainties are much more noticeable in FLACS than in FDS throughout the fire scenarios simulated. Therefore, the results found are far more reliable in FDS even if these are considerably inaccurate, while those obtained in FLACS may lead to erroneous conclusions when considered due to the significant fluctuations found.

Regardless of the combustibles involved and the boundary conditions, the agreements between the burning rates simulated and measured mostly depend on the pools diameter in both CFD tools (Figure 7b). In the case of FDS, more accurate mean burning rates are predicted as the pool diameter increases: 1.5 and 3 m-diameter pool fires have an over-estimation error slightly higher than 25%; whereas the rest of the fires modelled are identified with an estimation error lower than 25 %. Indeed, 5 m-diameter pools shows perfect agreement with measurements. Contrary, less accurate results are found as the pool diameter increases in FLACS: 1.5 and 3 m-diameter pools reach the highest mean burning rate agreements. Therefore, as the pools size increase in

FLACS simulations, the radiative heat from the flame considerably accelerates the liquid evaporation rate hence releasing a higher amount of vapor fuel than expected in reality.

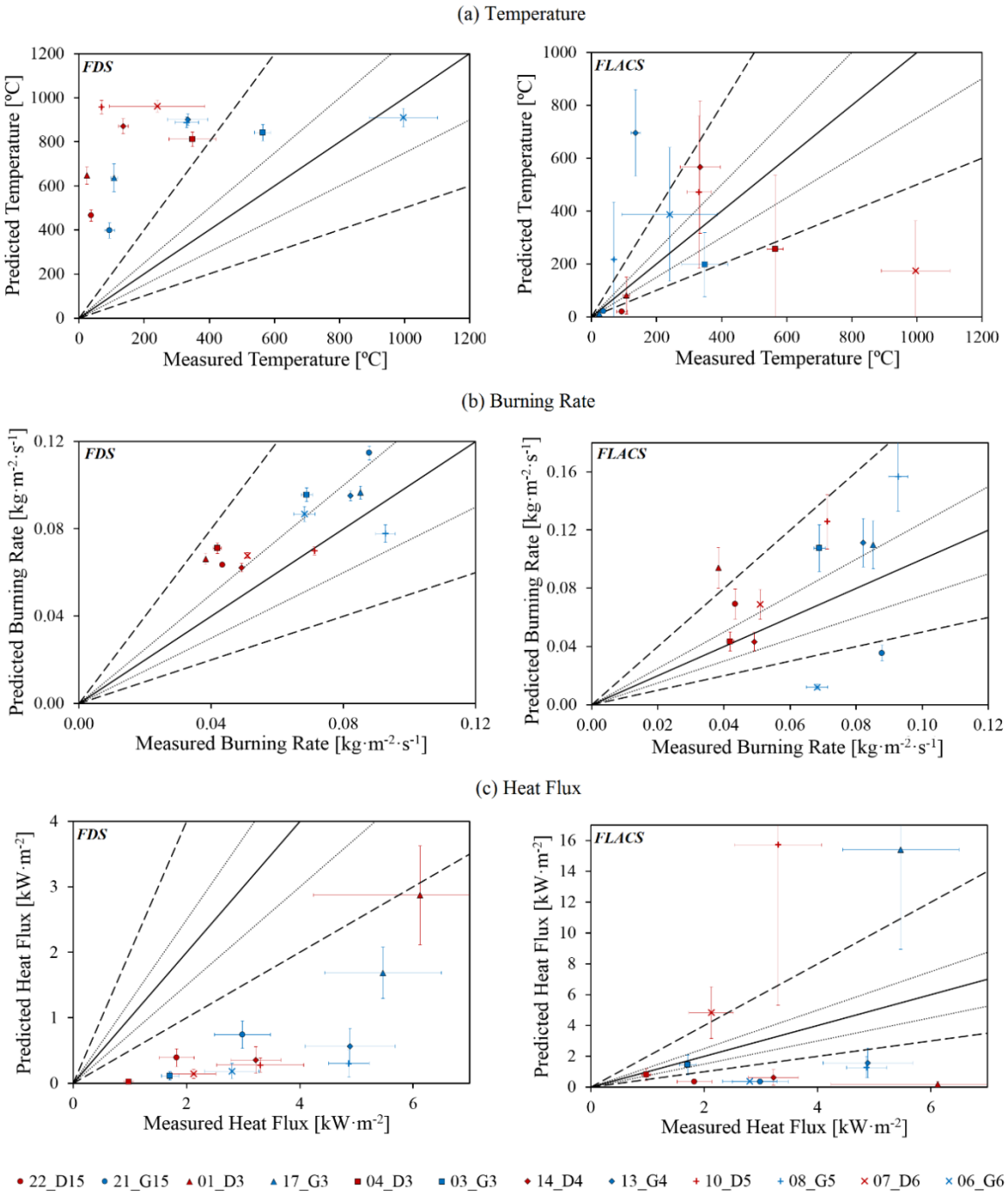

Figure 7. Forecast errors a) of the mean temperatures found along the different thermocouples; b) the mean burning rates registered; and c) the mean heat flux received by means of FDS and FLACS-Fire. Vertical and horizontal error bars indicate the uncertainties of the simulation results and measurements, respectively.

As a result of the low influence of the wind in the FDS simulations, the heat fluxes predicted are significantly under-estimated (Figure 7c). Apart from the 3 m-diameter pools in the absence of wind (04_D3 and 03_G3), whose heat fluxes are accurately predicted, the rest of the FLACS simulations also lead to considerable disagreements. This fact highlight the need to perform a detailed sensitivity analysis of different wind profiles and grid sizes under various scenarios in order to reveal the most appropriate modelling options for large-pool

fires. Indeed, *a posteriori* CFD simulations may contribute to that end and therefore, these may deliver more accurate estimations of the flame temperatures and heat fluxes received at a certain distance from the pool origin. Moreover, the radiation model applied in each code and the number of solid angles considered may also play an essential role in determining the radiative heat transfer within the computational domain. The FLACS simulations, which were run with the DTM approach, commonly deliver more accurate heat flux results in windless pool fires than FDS, whose simulations were run with the FVM approach. Accordingly, the DTM radiation model may provide more reliable results than the FVM in spite of the considerable results fluctuations found in FLACS.

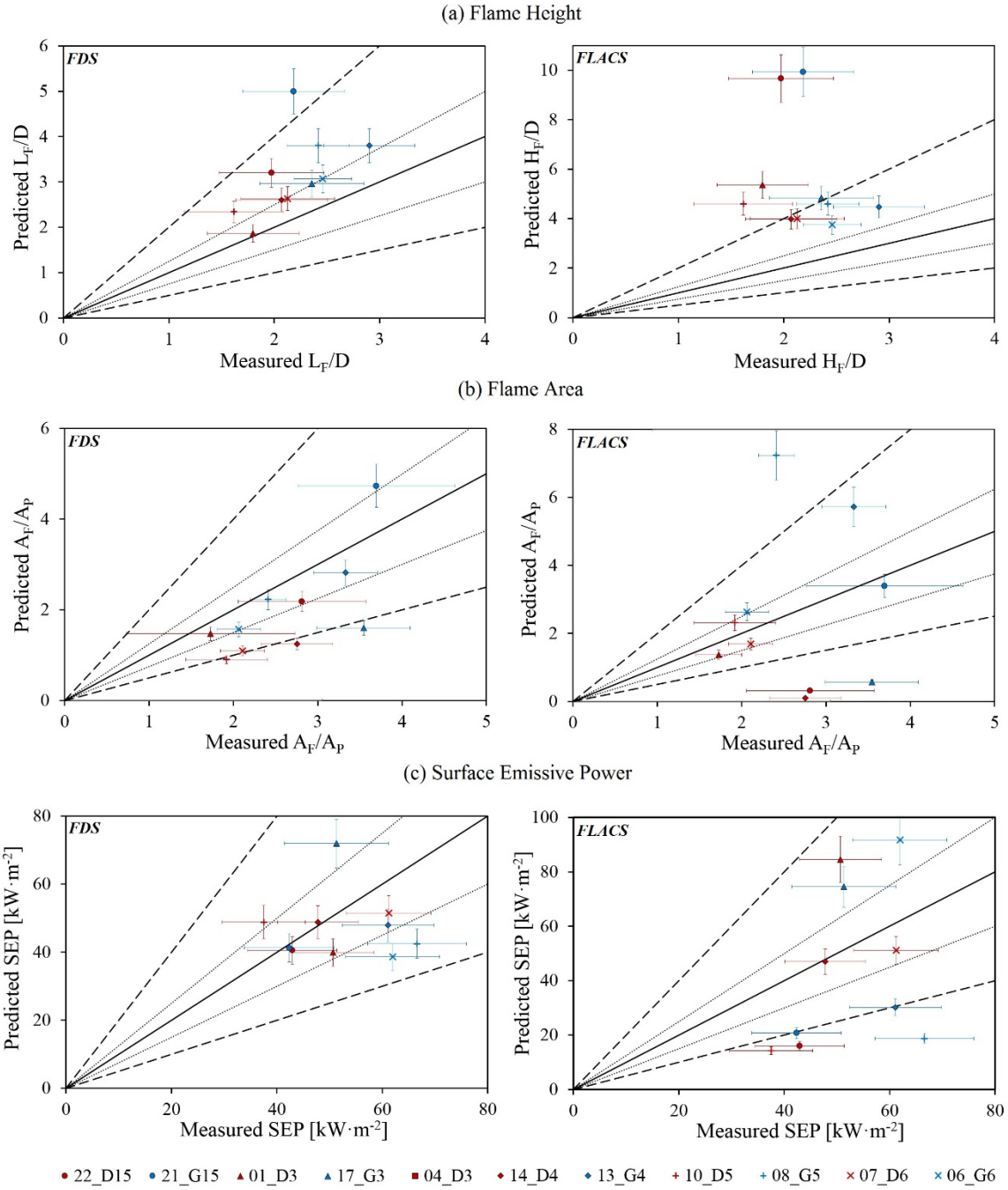

Figure 8. Forecast errors a) of the mean flame height; b) the mean flame area; and c) mean surface emissive power estimated by means of FDS and FLACS-Fire. Vertical and horizontal error bars indicate the uncertainties of the simulation results and measurements, respectively.

Figure 8 depicts the flame-geometry descriptors obtained by means of the numerical slice file that registered the mean flame temperature of the modelled pool fires during the steady state. Regarding the dimensionless mean flame heights, it is underlined that both CFD tools tend to slightly over-estimate the measured values (Figure 8a). Particularly, FDS is able to reasonably predict the flame heights measured except the 1.5 m-diameter gasoline pool. Differently, considerable over-predictions of the 1.5 m-diameter pools and the fire scenarios under wind velocities higher than 1 m·s^{-1} (01_D3 and 10_D5) are found in FLACS simulations. Consequently, it is highlighted that both CFD had difficulties in forecasting flame heights of 1.5 m-diameter pools as well as the notable influence of high wind speeds over FLACS results. On the other hand, good numerical agreement is found in the dimensionless mean flame areas modelled with FDS even though simulation results tend to under-predict the measured values (Figure 8b). Conversely, the wind velocity remarkably affects the mean flame areas obtained in FLACS regardless of the fire sizes. In general, as the flame gets tilted under considerable wind conditions, the flame height increases and the flame area decreases in both CFD codes. Nevertheless, the wind has a greater influence over the measurements analyzed in FLACS than in FDS. For example, in FLACS the 22_D15 fire experiment clearly over/under-estimates its flame height and area, respectively. Conversely, the same fire experiment in FDS shows a slight over/under-prediction of these variables. However, the mean surface emissive power derived from the FDS reasonably agree with measurements (Figure 8c). Apart from the 1.5 and 5 m-diameter pools, FLACS is able to forecast the SEP values of the rest of the pools simulated. In fact, the fires size results more important than the wind conditions or the liquid fuel in determining the SEP in both CFD codes.

4.2.2 Quantitative error estimation

Due to the difficulties in determining the suitability of each tool to predict the main fire behaviour variables according to the pool fires examined, two quantitative performance measures have been calculated: the fractional bias (FB) and the normalized mean square error (NMSE) (Muñoz et al., 2004). If a variable of interest has N number of predicted values X_p corresponding to the measurements found, X_0 then these statistics can be calculated as follows:

$$FB = \frac{1}{N}\sum_{1}^{N} 2\frac{X_0 - X_p}{X_0 + X_p} \quad (11)$$

$$NMSE = \frac{1}{N}\sum_{1}^{N} \frac{(X_0 - X_p)^2}{X_0 X_p} \quad (12)$$

The FB is a measure of the under or over-estimations of the model (negative/positive values indicates that the model over/under-estimates the results); whereas the NMSE is a measure of scatter and reflects the relative fit of a model to data. Simulation results will only agree with experimental measurements if both statistical methods are within the following performance criteria: the random scatter is about a factor of 2 of the mean (NMSE ≤ 0.5); and the mean bias is within ±30 % of the mean (-0.3 ≤ FB ≤ 0.3) (Mouilleau and Champassith, 2009). Table 4 summarizes the FB and NMSE measurements obtained from the large-scale pool fires simulated with FDS and FLACS where italic blue values indicate that the measurement is within the performance criteria established.

It can be clearly seen that the mean flame temperatures meet the performance criteria in the 8 % of the pool fires simulated in both CFD codes. Nevertheless, certain measuring errors could have been derived during the experiments as the thermocouples used were of 3 mm-diameter. Thinner thermocouples would have probably led to more accurate temperature results. In addition, it is noted that most of the flame temperatures are over-estimated in both CFD codes according to the FB results. Therefore, it is deduced that flames are less tilted than expected probably due to the low impact of the simulated wind profile over the fire behavior. Moreover, this phenomena also lead to under-predictions of the heat fluxes registered, as only the 17 % of the simulation results agree within the performance criteria in FLACS. On the other hand, the burning rates obtained with FDS comply within the criteria in the 75% of the cases, while the 42 % of the results are in accordance when modelled with FLACS. Particularly, the non-complying burning rates calculated in FLACS are usually higher than those measured, which may be due to the assumptions made within the heat transfer balance when it solves the liquid evaporation model.

Concerning the flame height results, the 60 % of the pool fires simulated with FDS agree with the established performance criteria. In fact, the discrepancies are commonly found when modelling pools of 1.5 and 5 m-diameter. Conversely, none of the pools modelled with FLACS meet the defined criteria, as the flame heights largely over-estimate the measured values. Moreover, the 60 % of the flame areas analysed with FDS agree within the criteria. In that case, the non-complying simulations are those concerning pools of 4, 5 and 6 m-diameter under wind speeds higher than 0.75 m·s^{-1}. Therefore, the simulated wind profile might be the main

responsible of these disagreements. On the other hand, only the 50 % of the simulations performed with FLACS meet the performance criteria. Apart from the errors led by the modelled wind profiles, the discrepancies found in FLACS may be also derived from the large cell sizes employed. Additionally, the fact of averaging the flow motion due to the RANS turbulence model may be crucial in determining the flame shape and temperature contour. In any case, it is pointed out that the methodology applied to assess the flame-shape features through a numerical slice file measuring the mean flame temperatures resulted generally satisfactory in FDS simulations, whereas it led to significant disagreements in FLACS. Furthermore, the 70 % and 20 % of the mean surface emissive power calculated are in accordance with the performance criteria in FDS and FLACS, respectively. Particularly, gasoline pool fires modelled with FDS in the absence of wind led to erroneous predictions as they may forecast higher flame temperatures than expected, while the low agreement of the SEP resulted in FLACS may be due to the erroneous flame heights predictions. The promising SEP results found in FDS demonstrate that the method implemented, which consisted on recording the irradiance in a perpendicular location to the wind direction, was successfully applied.

Table 4: FB and NMSE measurements of the main variables of interest obtained with the different CFD tools used for the large-pool fires simulated. Italic blue values indicate that the measurement is within the performance criteria established

Experiments	Flame Temperature		Burning Rate		Heat Flux		Flame Height		Flame Area		Surface Emissive Power	
	FDS	**FLACS**	**FDS**	**FLACS**	**FDS**	**FLACS**	**FDS**	**FLACS**	**FDS**	**FLACS**	**FDS**	**FLACS**
22_D15												
FB	-1.71	0.49	*-0.30*	-0.46	1.30	1.35	-0.47	-1.32	*0.25*	1.60	*0.06*	0.91
NMSE	10.9	0.26	*0.15*	0.22	3.36	3.45	0.24	3.10	*0.06*	6.99	*0.00*	1.05
21_G15												
FB	-1.23	1.28	*-0.26*	0.85	1.20	1.59	-0.78	-1.28	*-0.25*	*0.08*	*0.03*	0.68
NMSE	2.65	2.9	*0.07*	0.88	2.63	6.98	0.73	2.77	*0.06*	*0.01*	*0.00*	0.53
17_G3												
FB	-1.42	0.45	*-0.13*	*-0.25*	1.05	-0.87	*-0.23*	-0.69	0.76	1.44	-0.33	-0.37
NMSE	4.18	0.57	*0.02*	*0.06*	1.67	1.30	*0.05*	0.54	0.67	4.36	0.12	0.14
04_D3												
FB	-0.81	0.63	-0.52	*-0.04*	1.90	*0.28*	n/a	n/a	n/a	n/a	n/a	n/a
NMSE	0.87	1.41	0.29	*0.00*	49.2	*0.30*	n/a	n/a	n/a	n/a	n/a	n/a
03_G3												
FB	-0.39	1.00	-0.32	-0.44	1.76	*0.24*	n/a	n/a	n/a	n/a	n/a	n/a
NMSE	0.16	5.02	0.11	0.20	17.7	*0.25*	n/a	n/a	n/a	n/a	n/a	n/a
01_D3												
FB	-1.86	0.65	-0.53	-0.84	0.69	1.81	*-0.04*	-1.00	*0.16*	*0.23*	*0.24*	-0.50
NMSE	25.6	0.47	0.31	0.86	0.71	18.6	*0.00*	1.32	*0.03*	*0.05*	*0.06*	0.27
14_D4												
FB	-1.46	-1.32	*-0.23*	*0.13*	1.61	1.39	*-0.23*	-0.63	0.76	1.87	*-0.02*	*0.02*
NMSE	4.66	3.43	*0.06*	*0.02*	10.2	4.89	*0.05*	0.44	0.67	27.86	*0.00*	*0.00*
13_G4												
FB	-0.93	*-0.28*	*-0.15*	*-0.30*	1.59	1.08	*-0.27*	-0.43	*0.17*	-0.53	*0.24*	0.68
NMSE	1.17	*0.48*	*0.02*	*0.09*	8.52	3.75	*0.07*	0.19	*0.03*	0.30	*0.06*	0.52
10_D5												
FB	-1.73	-0.58	*0.02*	-0.55	1.68	-1.06	-0.36	-0.96	0.72	*-0.19*	*-0.26*	0.90
NMSE	12.0	1.73	*0.00*	0.33	11.6	3.58	0.14	1.20	0.60	*0.03*	*0.07*	1.01
08_G5												
FB	-0.92	-0.13	*0.18*	-0.52	1.77	1.22	-0.45	-0.62	*0.08*	-1.00	0.44	1.12
NMSE	1.10	1.09	*0.04*	0.29	22.6	3.45	0.21	0.43	*0.01*	1.33	0.21	1.83
07_D6												
FB	-1.24	-0.64	*-0.28*	*-0.30*	1.74	-0.74	*-0.21*	-0.61	0.63	*0.22*	*0.17*	*0.18*
NMSE	3.56	1.81	*0.08*	*0.09*	15.3	0.83	*0.05*	0.41	0.44	*0.05*	*0.03*	*0.03*
06_G6												
FB	*0.09*	1.48	*-0.24*	1.39	1.75	1.54	*-0.22*	-0.42	*0.27*	*-0.24*	0.46	-0.39
NMSE	*0.02*	15.5	*0.06*	3.72	19.4	6.06	*0.05*	0.18	*0.08*	*0.06*	0.23	0.16

5. Conclusions

The predictive capabilities of FDS and FLACS-Fire were examined when forecasting the main fire variables (i.e. flame temperatures, burning rates, heat fluxes, flame heights, flame areas and surface emissive powers) of unconfined large-scale hydrocarbon fires of different sizes: 1.5, 3, 4, 5 and 6 m-diameter. During the experiments, it was commonly observed that the main variables of interest reached greater values with gasoline fuel than with diesel. The boundary conditions and the pool diameter resulted crucial factors in the overall variables analysed. Indeed, the mean flame temperatures widely varied depending on the wind velocity and the pool size as the flames could be significantly tilted. Then, it was also found that the resulting burning rates increased as the fire size and the wind velocity augmented. However, the heat fluxes received at a certain distance from the fire origin decreased as the pool diameter augmented, while it increased as the wind velocity augmented. The dimensionless flame heights remained approximately steady throughout the different experiments performed; the dimensionless flame areas diminished as the diameter increased and varied depending on the fuel involved and the wind speed; the SEP increased as the diameter augmented and as the flame area, the values varied depending on the fuel involved and the wind speed.

Qualitative assessment of the predictions and quantitative statistical measures were carried out in order to determine the suitability of each tool to predict the harmful fire effects when performing *a priori* CFD simulations. In general, temperatures were over-estimated as the flames were usually higher and less tilted than in experiments due to the difficulty in modelling wind entrainment. Consequently, numerous discrepancies were found when comparing the heat fluxes simulated and measured in both tools. On the other hand, accurate burning rate results were commonly found in FDS, while less accurate ones were obtained in FLACS as the diameter increased. Additionally, the flame-geometry descriptors were determined through a 2D slice file on the pool central axis that numerically registered the mean flame temperatures and a radiometer located perpendicular to the wind direction to measure the irradiancy. In general, the flame heights found were slightly over-estimated in both tools, as a result of the low impact of the wind velocity over the flame behaviour. Then, both the flame area and the SEP calculated with FDS revealed good agreement with the experiments, while FLACS delivered a wide variety of results that under/over-estimated the measured data. Therefore, it is stated that the method applied to determine the flame-geometry descriptors resulted generally satisfactory in FDS simulations, whereas it led to significant disagreements in FLACS. Furthermore, it is remarked that the simulation results found in FDS are far more reliable than those obtained in FLACS, which may lead to erroneous conclusions when considered, due to the significant uncertainties achieved around the mean values.

The results presented in this paper show the great potential of CFD tools to forecast the main fire effects of large-sale hydrocarbon fires. It has been demonstrated that these modelling tools may be perfectly used to perform risk analysis in chemical and process industries in order to determine the measures that should be implemented to prevent major fire accidents. However, a more comprehensive study is still needed to figure out the sub-models influence over the resulting pool fires simulated. Actually, a detailed sensitivity analysis might reveal the most appropriate modelling options (i.e. the wind profile, the mesh resolutions and the number of solid angles). To that end, *a posteriori* simulations should be undertaken and CFD validation guidelines could be developed to guarantee the correctness of the validation process performed. Furthermore, it would be of great interest to expand the current validation analysis to higher pool fire diameters. Finally, comparisons between data collected in this paper together with data from simplified fire modelling tools may determine the most suitable approach when predicting the pools fire related-effects.

Acknowledgments

Spanish Ministry of Economy and Competitiveness (project CTM2014-57448-R, co-financed with FEDER funds), Spanish Ministry of Education, Culture and Sport (FPI Program) and Autonomous Government of Catalonia (Project No. 2014-SGR-413).

References

Audouin, L., Kolb, G., Torero, J.L., Most, J.M., 1995. Average Centreline Temperatures of a Buoyant Pool Fire Obtained by Image Processing of Video Recordings. Fire Saf. J. 24, 167–187.

Azzi, C., Rogstadkjenet, L., 2016. Use of CFD in the Performance-Based Design for Fire Safety in the Oil and Gas Sector, in: 11th Conference on Performance-Based Codes and Fire Safety Design Methods.

Baalisampang, T., Abbassi, R., Garaniya, V., Khan, F., Dadashzadeh, M., 2017. Modelling the Impacts of Fire in a Typical FLNG Processing Facility, in: International Conference on Safety and Fire Engineering.

Calvo Olivares, R.D., Rivera, S.S., McLeod, J.E., 2015. Database for accidents and incidents in the fuel ethanol industry. J. Loss Prev. Process Ind. 38, 276–297. https://doi.org/10.1016/j.jlp.2015.10.008
Calvo Olivares, R.D., Rivera, S.S., McLeod, J.E., 2014. Database for accidents and incidents in the biodiesel industry. J. Loss Prev. Process Ind. 29, 245–261. https://doi.org/10.1016/j.jlp.2014.03.010
Casal, J., 2017. Evaluation of the Effects and Consequences of Major Accidents in Industrial Plants. 2nd ed. Elsevier, Amsterdam.
Chai, J., Lee, H., Patankar, S., 1994. Finite Volume Method for Radiation Heat Transfer. J. Thermophys. Heat Transf. 8, 419–425.
Chatris, J.M., Quintela, J., Folch, J., Planas, E., Arnaldos, J., Casal, J., 2001. Experimental study of burning rate in hydrocarbon pool fires. Combust. Flame 126, 1373–1383. https://doi.org/10.1016/S0010-2180(01)00262-0
Cowley, L.T., Johnson, A.D., 1991. Blast and fire engineering project for topside structures. Fire loading series.
Cox, G., Chitty, R., 1980. A Study of the Deterministic Properties of Unbounded Fire Plumes. Combust. Flame 39, 191–209.
Ferrero, F., Muñoz, M., Arnaldos, J., 2007. Effects of thin-layer boilover on flame geometry and dynamics in large hydrocarbon pool fires. Fuel Process. Technol. 88, 227–235. https://doi.org/10.1016/j.fuproc.2006.09.005
Ferrero, F., Muñoz, M., Kozanoglu, B., Casal, J., Arnaldos, J., 2006. Experimental study of thin-layer boilover in large-scale pool fires. J. Hazard. Mater. 137, 1293–1302. https://doi.org/10.1016/j.jhazmat.2006.04.050
FLACS v10.5 User's Manual, 2016.
Floyd, J., Baum, H., McGrattan, K., 2001. A Mixture Fraction Combustion Model for Fire Simulation using CFD, in: International Conference on Engineered Protection Design. pp. 279–290.
Fu, S., Yan, X., Zhang, D., Li, C., Zio, E., 2016. Framework for the quantitative assessment of the risk of leakage from LNG-fueled vessels by an event tree-CFD. J. Loss Prev. Process Ind. 43, 42–52. https://doi.org/10.1016/j.jlp.2016.04.008
Guidance on Risk Assessment for Offshore Installations, 2006.
Jones, W.P., Launder, B.., 1972. The prediction of laminarization with a two-equation model of turbulence. Int. J. Heat Mass Transf. 15, 301–314. https://doi.org/10.1016/0017-9310(72)90076-2
Koseki, H., 1999. Large Scale Pool Fires: Results of Recent Experiments, in: Fire Safety Science - Proceedings of the Sixth International Symposium. pp. 115–132.
Lin, C., Ferng, Y., Hsu, W., Hua, N.T., 2010. Investigations on the Characteristics of Radiative Heat Transfer in Liquid Pool Fires. Fire Technol. 46, 321–345. https://doi.org/10.1007/s10694-008-0071-7
Magnussen, B., Hjertager, B., 1977. On mathematical modeling of turbulent combustion with special emphasis on soot formation and combustion. Symp. Combust. 16, 719–729. https://doi.org/10.1016/S0082-0784(77)80366-4
Maragkos, G., Beji, T., Merci, B., 2017. Advances in modelling in CFD simulations of turbulent gaseous pool fires. Combust. Flame 181, 22–38. https://doi.org/10.1016/j.combustflame.2017.03.012
McGrattan, K., Hostikka, S., McDermott, R., Floyd, J., Weinschenk, C., Overholt, K., 2015. Fire Dynamics Simulator User's Guide. https://doi.org/10.6028/NIST.SP.1019
McGrattan, K., Miles, S., 2016. Modeling Fires Using Computational Fluid Dynamics (CFD), in: Hurley, M. (Ed.), SFPE Handbook of Fire Protection Engineering. pp. 1034–1065. https://doi.org/10.1007/978-1-4939-2565-0
Mishra, K.B., 2010. Experimental investigation and CFD simulation of organic peroxide pool fi res (TBPB and TBPEH). Universität Duisburg-Essen.
Möller, F., 1973. Einführung in die Meteorologie. Mannheim, Germany.
Monin, A., Obukhov, A., 1959. Basic laws of turbulent mixing in the surface layer of the atmosphere. Tr. Akad. Nauk SSSR Geophiz. Inst. 24, 163–187.
Mouilleau, Y., Champassith, A., 2009. CFD simulations of atmospheric gas dispersion using the Fire Dynamics Simulator (FDS). J. Loss Prev. Process Ind. 22, 316–323. https://doi.org/10.1016/j.jlp.2008.11.009
Muñoz, M., Arnaldos, J., Casal, J., Planas, E., 2004. Analysis of the geometric and radiative characteristics of hydrocarbon pool fires. Combust. Flame 139, 263–277. https://doi.org/10.1016/j.combustflame.2004.09.001
Muñoz, M., Planas, E., Ferrero, F., Casal, J., 2007. Predicting the emissive power of hydrocarbon pool fires. J. Hazard. Mater. 144, 725–729. https://doi.org/10.1016/j.jhazmat.2007.01.121
Pedersen, N., 2012. Modeling of jet and pool fires and validation of the fire model in the CFD code FLACS.
Planas-Cuchi, E., Chatris, J., López, C., Arnaldos, J., 2003. Determination of flame emissivity in hydrocarbon pool fires using infrared thermography. Fire Technol. 39, 261–273. https://doi.org/10.1023/A:1024193515227
Pula, R., Khan, F.I., Veitch, B., Amyotte, P.R., 2005. Revised fire consequence models for offshore quantitative risk assessment. J. Loss Prev. Process Ind. 18, 443–454. https://doi.org/10.1016/j.jlp.2005.07.014
Sally, M., Kassawara, R., 2007. NUREG-1824. Verification and Validation of Selected Fire Models for Nuclear Power Plant Applications.
Sapa, B., Plion, P., Gay, L., Nmira, F., Wang, H.Y., 2010. On the numerical modeling of buoyancy-dominated turbulent diffusion flames by using URANS with a k-e turbulence model. Combust. Sci. Technol. 176,

1007–1034. https://doi.org/10.1080/00102200490428602
Shah, N., 1979. A new method of computation of radiation heat transfer in combustion chambers. Imperial College, University of London.
Sikanen, T., Hostikka, S., 2017. Predicting the heat release rates of liquid pool fires in mechanically ventilated compartments. Fire Saf. J. 0–1. https://doi.org/10.1016/j.firesaf.2017.03.060
Sikanen, T., Hostikka, S., 2016. Modeling and simulation of liquid pool fires with in-depth radiation absorption and heat transfer. Fire Saf. J. 80, 95–109. https://doi.org/10.1016/j.firesaf.2016.01.002
Smagorinsky, J., 1963. General circulation experiments with the primitive equations. I: The basic experiment. Mon. Weather Rev. 91, 99–165.
Sudheer, S., 2013. Characterization of Open Pool Fires and Study of Heat Transfer in Bodies Engulfed in Pool Fires.
Torero, L., Jahn, W., Stern-gottfried, J., Ryder, N.L., Rein, G., Mowrer, F., Coles, A., Joyeux, D., Desanghere, S., La, M., Alvear, D., Capote, J.A., Jowsey, A., Abecassis-empis, C., Reszka, P., 2009. Round-robin study of a priori modelling predictions of the Dalmarnock Fire Test One. Fire Saf. J. 44, 590–602. https://doi.org/10.1016/j.firesaf.2008.12.008
Vasanth, S., Tauseef, S.M., Abbasi, T., Abbasi, S.A., 2013. Assessment of four turbulence models in simulation of large-scale pool fires in the presence of wind using computational fluid dynamics (CFD). J. Loss Prev. Process Ind. 26, 1071–1084. https://doi.org/10.1016/j.jlp.2013.04.001
Vianna, S., Huser, A., 2010. Fire CFD modelling applied to offshore design, in: FIRESEAT. pp. 65–76.
Wahlqvist, J., Hees, P. Van, 2016. Implementation and validation of an environmental feedback pool fire model based on oxygen depletion and radiative feedback in FDS. Fire Saf. J. 85, 35–49. https://doi.org/10.1016/j.firesaf.2016.08.003

a) VHS Camera

b) IR Camera

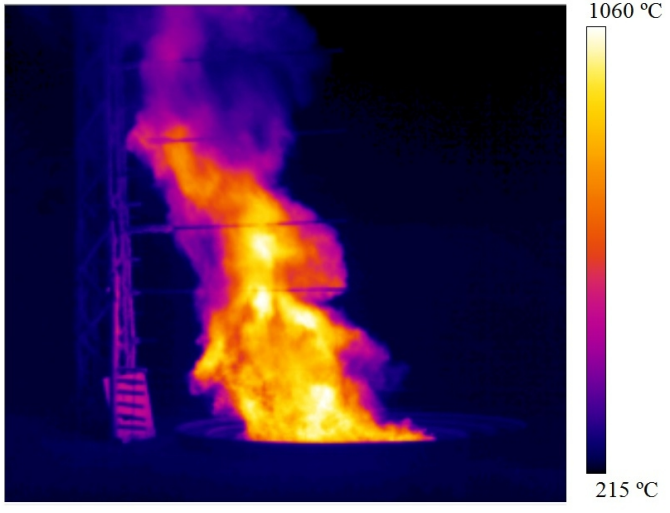

c) Segmented Image

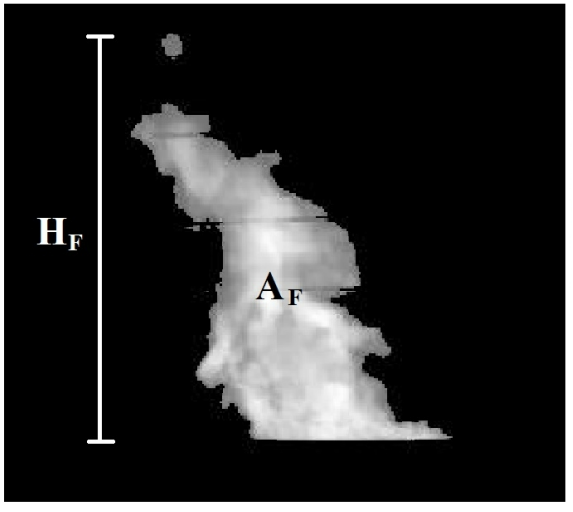

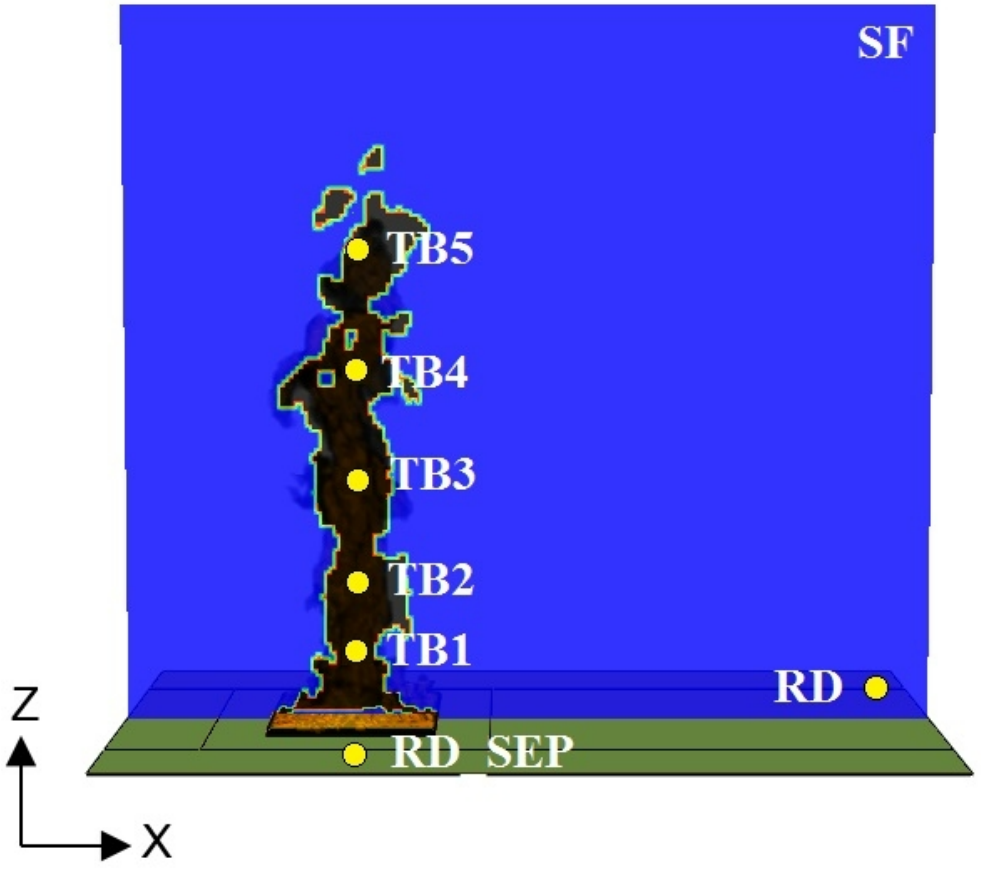
SF
TB5
TB4
TB3
TB2
TB1
RD
RD_SEP
Z
X

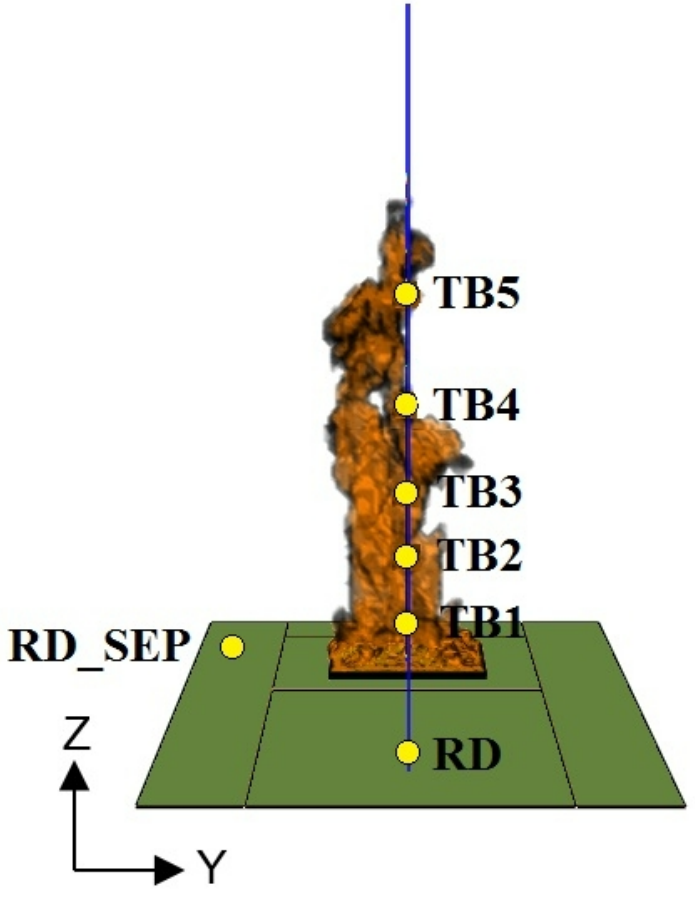
TB5
TB4
TB3
TB2
TB1
RD_SEP
RD
Z
Y

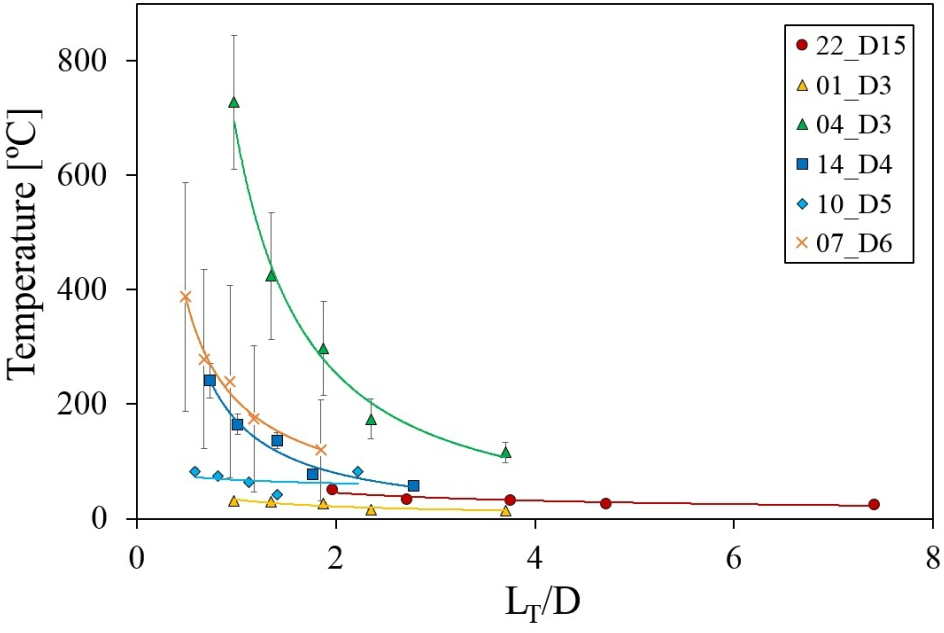
Temperature [ºC]
0
200
400
600
800
0
2
4
6
8
L_T/D
22_D15
01_D3
04_D3
14_D4
10_D5
07_D6

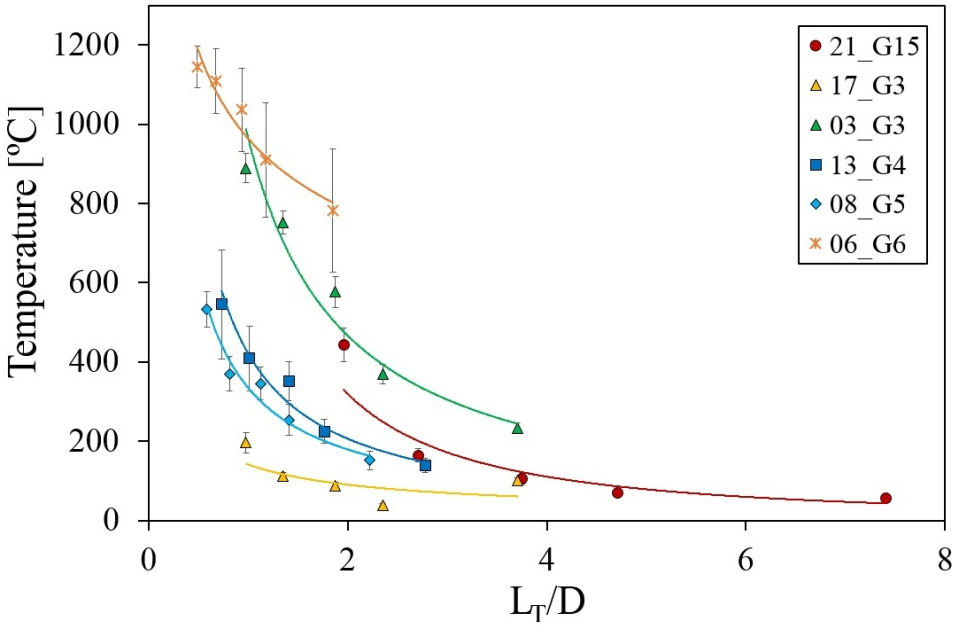
Temperature [ºC]
0
200
400
600
800
1000
1200
0
2
4
6
8
L_T/D
21_G15
17_G3
03_G3
13_G4
08_G5
06_G6

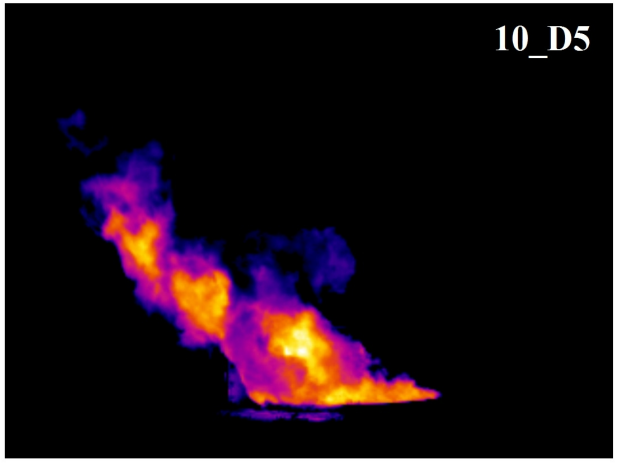
10_D5

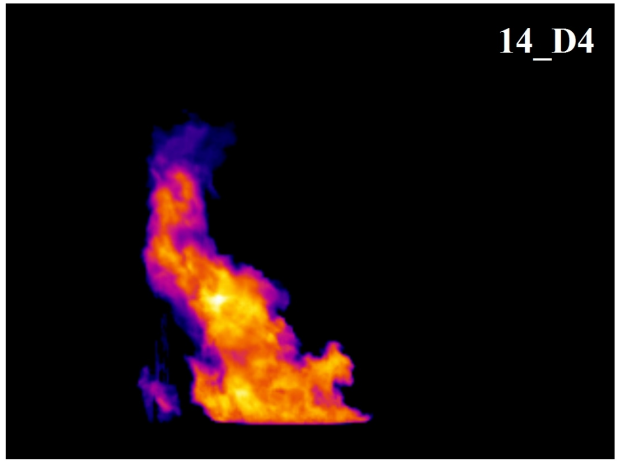
14_D4

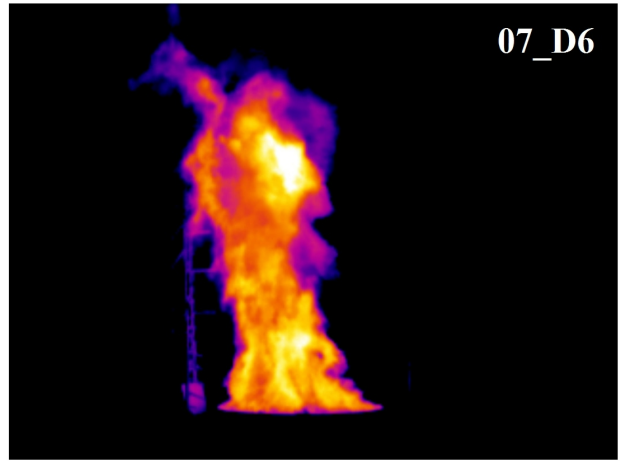
07_D6

(a) Burning Rate

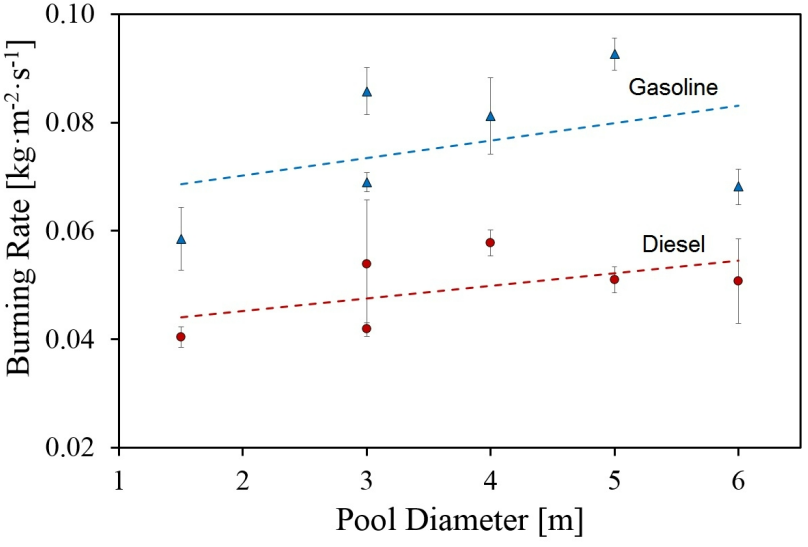

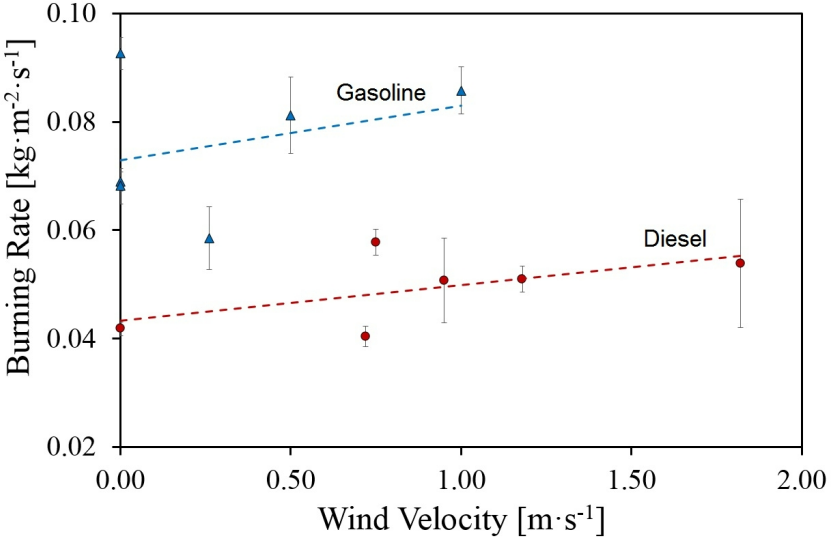

(b) Heat Flux

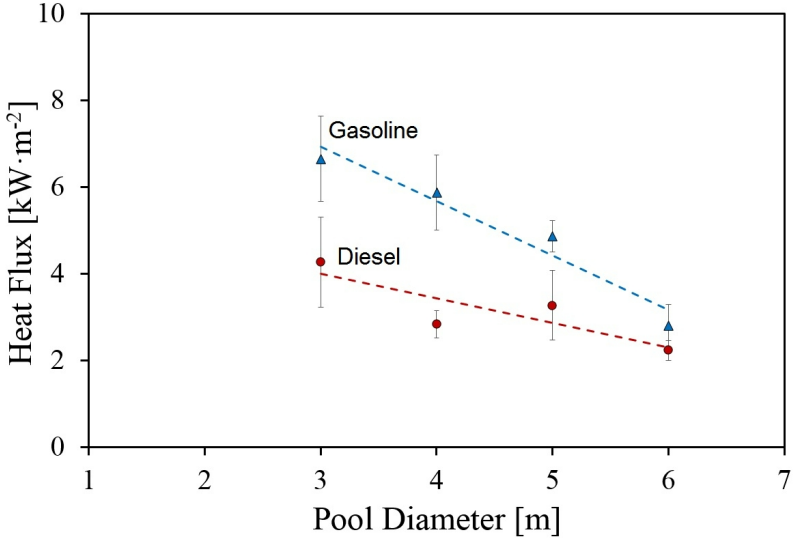

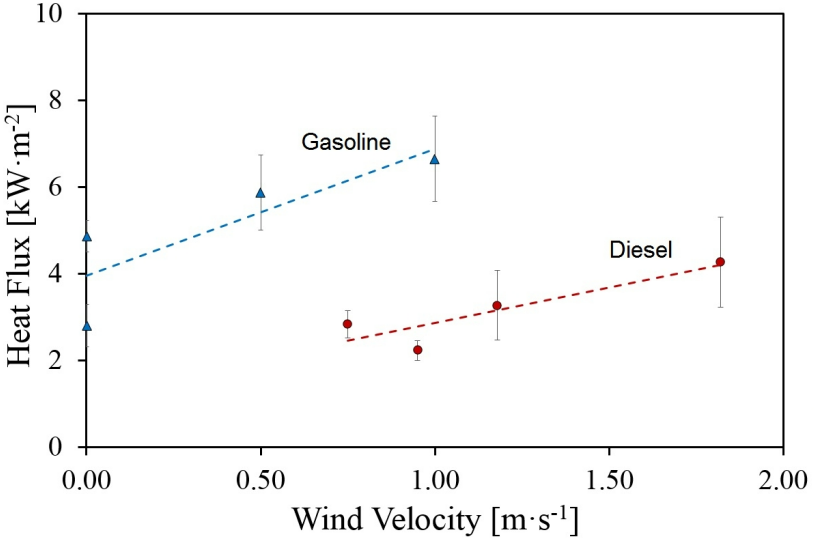

(a) Flame Length

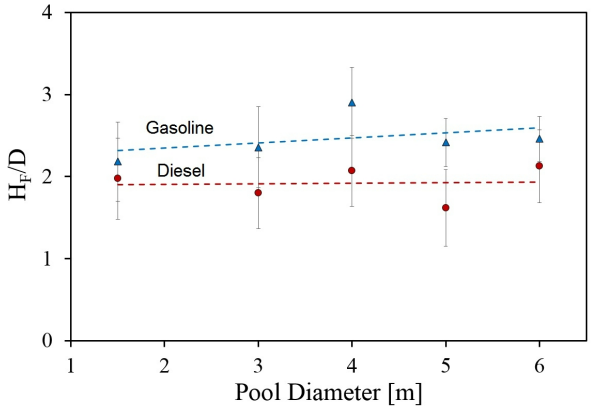

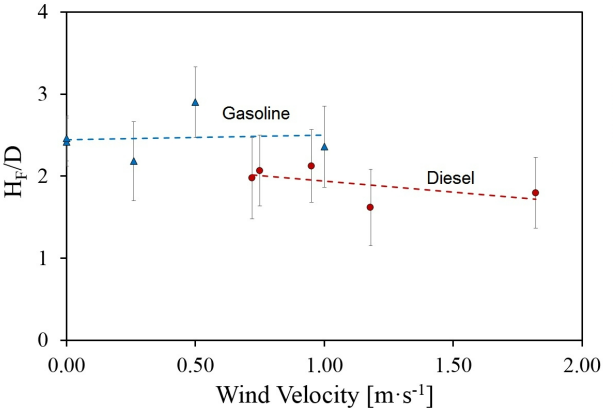

(b) Flame Area

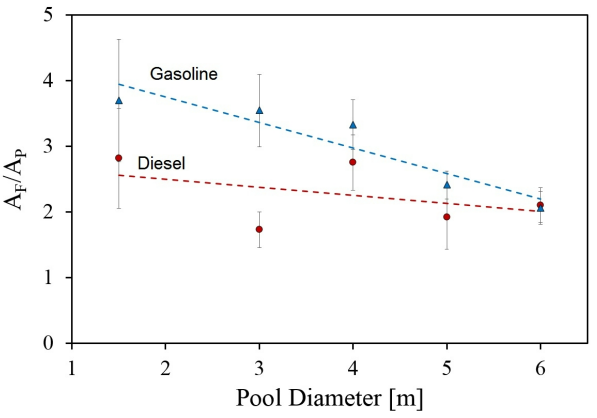

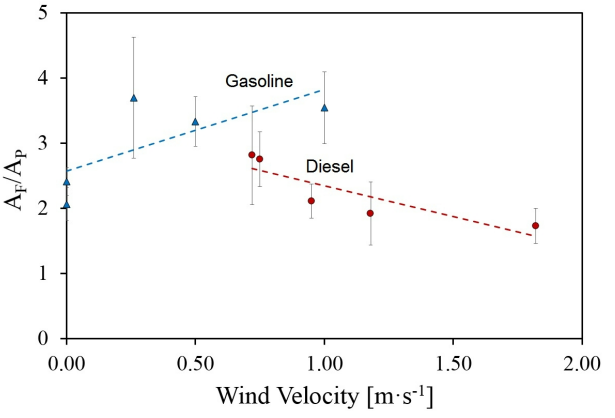

(c) Surface Emissive Power

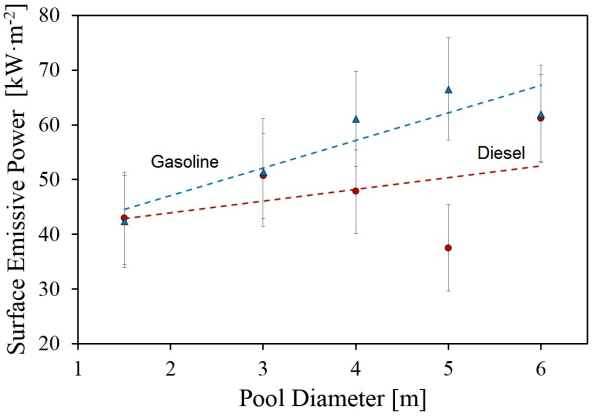

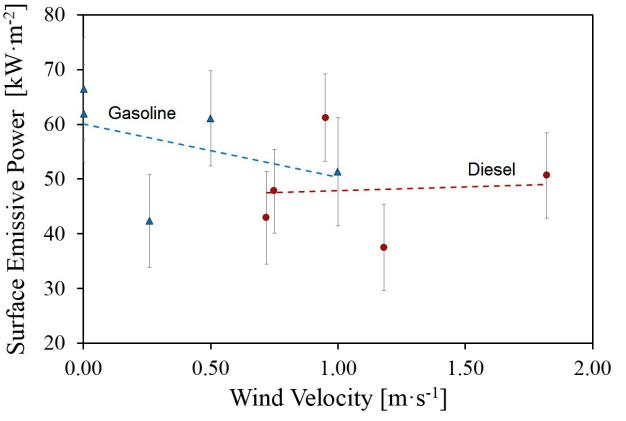

(a) Temperature

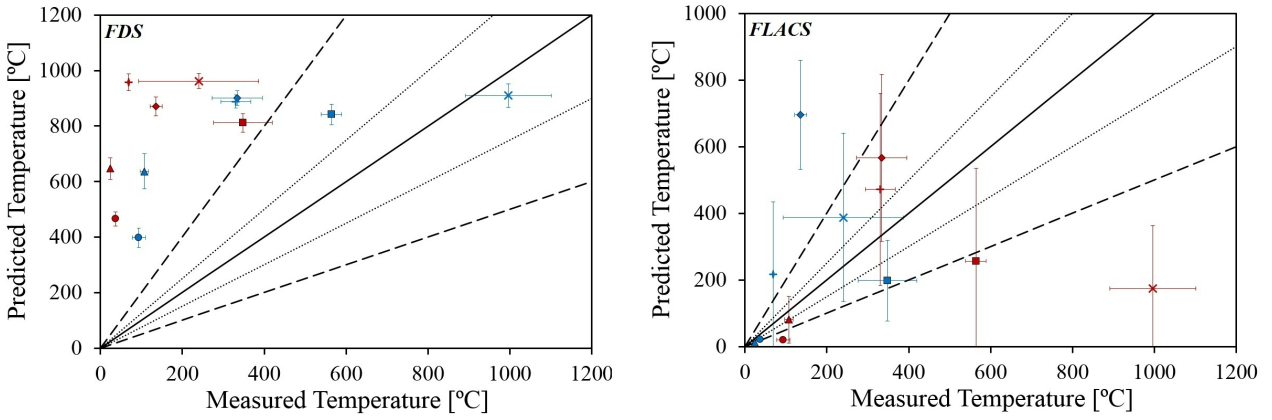

(b) Burning Rate

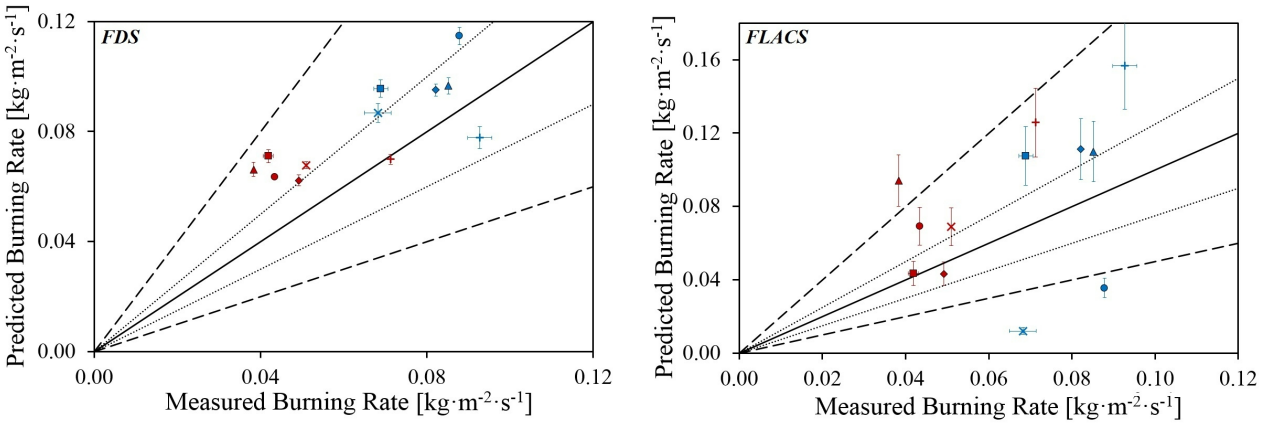

(c) Heat Flux

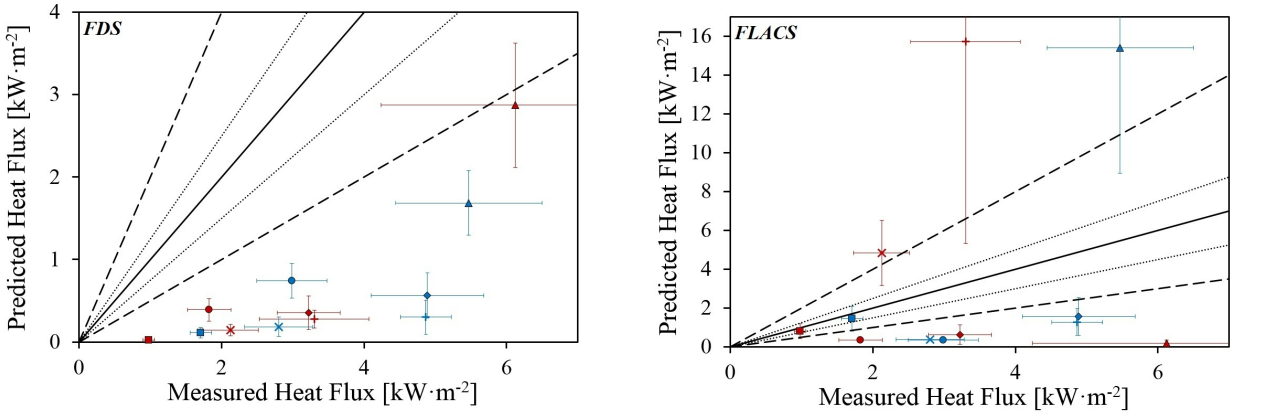

(a) Flame Height

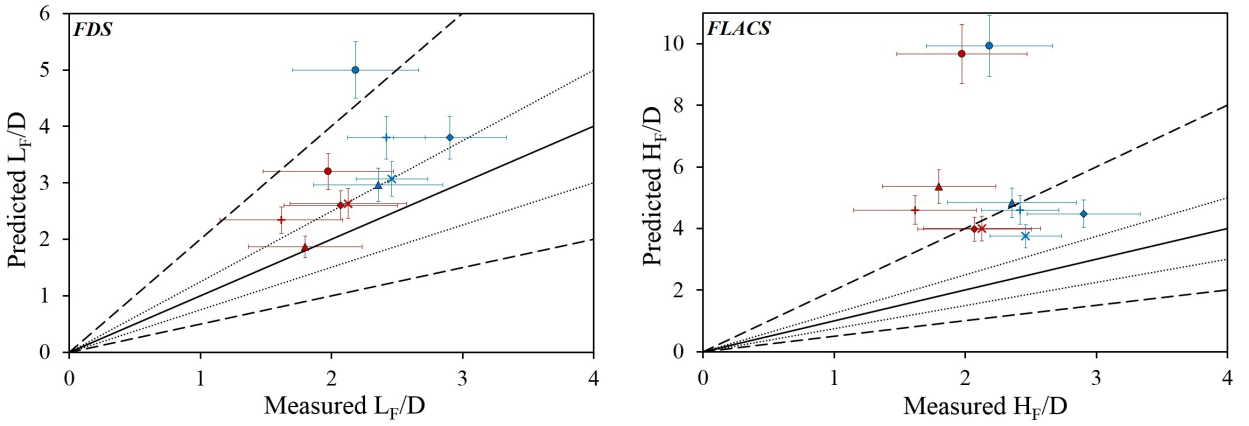

(b) Flame Area

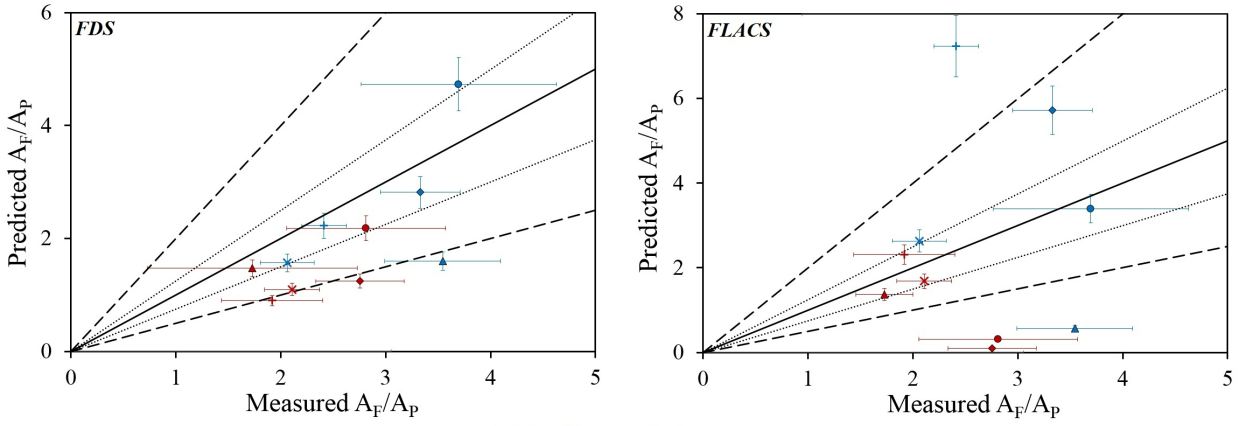

(c) Surface Emissive Power